

## TITLE

Modeling Alzheimer's disease using iPSCs reveals stress phenotypes associated with intracellular A $\beta$  and differential drug responsiveness

## AUTHOR LIST

**Takayuki Kondo,<sup>1,2,7</sup> Masashi Asai,<sup>7,9,10</sup> Kayoko Tsukita,<sup>1,7</sup> Yumiko Kutoku,<sup>11</sup> Yutaka Ohsawa,<sup>11</sup> Yoshihide Sunada,<sup>11</sup> Keiko Imamura,<sup>1</sup> Naohiro Egawa,<sup>1</sup> Naoki Yahata,<sup>1</sup> Keisuke Okita,<sup>1</sup> Kazutoshi Takahashi,<sup>1</sup> Isao Asaka,<sup>1</sup> Takashi Aoi,<sup>1</sup> Akira Watanabe,<sup>1</sup> Kaori Watanabe,<sup>7,10</sup> Chie Kadoya,<sup>7,10</sup> Rie Nakano,<sup>7,10</sup> Dai Watanabe,<sup>3</sup> Kei Maruyama,<sup>9</sup> Osamu Hori,<sup>12</sup> Satoshi Hibino,<sup>13</sup> Tominari Choshi,<sup>13</sup> Tatsutoshi Nakahata,<sup>1</sup> Hiroyuki Hioki,<sup>4</sup> Takeshi Kaneko,<sup>4</sup> Motoko Naitoh,<sup>5</sup> Katsuhiko Yoshikawa,<sup>5</sup> Satoko Yamawaki,<sup>5</sup> Shigehiko Suzuki,<sup>5</sup> Ryuji Hata,<sup>14</sup> Shu-ichi Ueno,<sup>15</sup> Tsuneyoshi Seki,<sup>16</sup> Kazuhiro Kobayashi,<sup>16</sup> Tatsushi Toda,<sup>16</sup> Kazuma Murakami,<sup>6</sup> Kazuhiro Irie,<sup>6</sup> William L. Klein,<sup>17</sup> Hiroshi Mori,<sup>18</sup> Takashi Asada,<sup>19</sup> Ryosuke Takahashi,<sup>2</sup> Nobuhisa Iwata,<sup>7,10,\*\*</sup> Shinya Yamanaka,<sup>1,8</sup> and Haruhisa Inoue<sup>1,7,8,\*</sup>**

<sup>1</sup>Center for iPS Cell Research and Application (CiRA)

<sup>2</sup>Department of Neurology, Graduate School of Medicine

<sup>3</sup>Department of Biological Sciences, Graduate School of Medicine and Department of Molecular and Systems Biology, Graduate School of Biostudies

<sup>4</sup>Department of Morphological Brain Science, Graduate School of Medicine

<sup>5</sup>Department of Plastic and Reconstructive Surgery, Graduate School of Medicine

<sup>6</sup>Organic Chemistry in Life Science, Division of Food Science and Biotechnology, Graduate School of Agriculture

Kyoto University, Kyoto 606-8507, Japan

<sup>7</sup>CREST

<sup>8</sup>Yamanaka iPS Cell Special Project

Japan Science and Technology Agency, Kawaguchi, Saitama 332-0012, Japan

<sup>9</sup>Department of Pharmacology, Faculty of Medicine, Saitama Medical University, Saitama 350-0495, Japan

<sup>10</sup>Division of Molecular Biology and Biotechnology, Department of Molecular Medicinal Sciences, Graduate School of Biomedical Sciences, Nagasaki University, Nagasaki 852-8521, Japan

<sup>11</sup>Department of Neurology, Kawasaki Medical School, Kurashiki, Okayama 701-0192, Japan

<sup>12</sup>Department of Neuroanatomy (Biotargeting), Kanazawa University Graduate School of Medical Sciences, Kanazawa, Ishikawa 920-8640, Japan

<sup>13</sup>Faculty of Pharmacy and Pharmaceutical Sciences, Fukuyama University, Fukuyama, Hiroshima 729-0292, Japan

<sup>14</sup>Department of Functional Histology

<sup>15</sup>Department of Psychiatry

Ehime University Graduate School of Medicine, Toon, Ehime 791-0295, Japan

<sup>16</sup>Division of Neurology/Molecular Brain Science, Kobe University Graduate School of Medicine, Kobe, Hyogo 650-0017, Japan

<sup>17</sup>Department of Neurobiology, Northwestern University, Evanston, IL 60208, USA

<sup>18</sup>Department of Neuroscience, Graduate School of Medicine, Osaka City University, 1-4-3 Osaka 545-8585, Japan

<sup>19</sup>Department of Neuropsychiatry, Institute of Clinical Medicine, Tsukuba University, Ibaraki 305-8577, Japan

\*Correspondence: haruhisa@cira.kyoto-u.ac.jp (H.I.)

\*\*Correspondence: iwata-n@nagasaki-u.ac.jp (N.I.)

Corresponding author 1

Haruhisa Inoue

email: haruhisa@cira.kyoto-u.ac.jp

TEL (+81)-75-366-7036

FAX (+81)-75-366-7094

Corresponding author 2

Nobuhisa Iwata

email: iwata-n@nagasaki-u.ac.jp

TEL & FAX (+81)-95-819-2435

**RUNNING TITLE**

Modeling Alzheimer's disease using patient iPSCs

**SUMMARY**

Oligomeric forms of amyloid- $\beta$  peptide ( $A\beta$ ) are thought to play a pivotal role in the pathogenesis of Alzheimer's disease (AD), but the mechanism involved is still unclear. Here we generated induced pluripotent stem cells (iPSCs) from familial and sporadic AD patients and differentiated them into neural cells.  $A\beta$  oligomers accumulated in iPSC-derived neurons and astrocytes in cells from patients with a familial amyloid precursor protein (APP)-E693 $\Delta$  mutation and sporadic AD, leading to endoplasmic reticulum and oxidative stress. The accumulated  $A\beta$  oligomers were not proteolytically resistant, and docosahexaenoic acid (DHA) treatment alleviated the stress responses in the AD neural cells. Differential manifestation of ER stress and DHA responsiveness may help explain variable clinical results obtained using DHA treatment and suggests that DHA may in fact be effective for a subset of patients. It also illustrates how patient-specific iPSCs can be useful for analyzing AD pathogenesis and evaluating drugs.

**HIGHLIGHTS**

1. Sporadic and familial Alzheimer's patient iPSCs-derived neural cells were analyzed.
2. Intracellular  $A\beta$  oligomers accumulate in lines from some patients
3.  $A\beta$  oligomers accumulation associated with ER and oxidative stress
4. DHA-alleviated ER- and oxidative stresses and improved cell viability

**INTRODUCTION**

Alzheimer's disease (AD) is the most prevalent neurodegenerative disorder. One of the pathological features of AD is oligomerization and aggregation and accumulation of amyloid  $\beta$  peptide ( $A\beta$ ), forming amyloid plaques in the brain. Cognitive impairment observed in clinical AD is inversely well correlated with the amount of  $A\beta$  oligomers in the soluble fraction, rather than the amount of  $A\beta$  fibrils (amyloid plaques) constituting them

(Haass and Selkoe, 2007; Krafft et al., 2010). Increasing evidence has shown that A $\beta$  oligomers extracted from AD-model mice or made from synthetic peptide cause neurotoxicity and cognitive impairments *in vitro* and *in vivo* (Walsh et al., 2002; Gong et al., 2003; Lesné et al., 2006), and this was also true in humans (Kuo et al., 2006; Shankar et al., 2008; Noguchi et al., 2009). Therefore, the formation and accumulation of A $\beta$  oligomers have been presumed to play a central role in the pathogenesis and clinical symptoms of AD.

A $\beta$ s are composed of 39-43 amino acid residues in length and are generated from amyloid precursor protein (APP) by  $\beta$ - and  $\gamma$ -secretase-mediated sequential cleavages. A number of mutations linked to familial AD in *APP* gene have been identified. Recently, an atypical early-onset familial AD, caused by E693 $\Delta$  mutation of APP producing variant A $\beta$  lacking 22nd Glu, was discovered in Japan (Tomiya et al., 2008). This APP-E693 $\Delta$  mutation presents rare, autosomal recessive mutations of *APP* gene related to familial AD. Patients with the mutation show early-onset overt symptoms of AD but lack A $\beta$  deposition according to PET scan analysis with a [ $^{11}$ C] Pittsburgh compound-B (PIB) radioprobe (Tomiya et al., 2008; Shimada et al., 2011). The 22nd Glu within the A $\beta$  sequence has a destabilizing effect on the formation of oligomeric structures due to electrostatic repulsion between the adjacent side chain of 22nd Glu (Kassler et al., 2010), and deletion of the amino acid residue leads to the ready formation of A $\beta$  oligomers *in vitro* (Nishitsuji et al., 2009). APP-E693 $\Delta$  transgenic mice show AD-like pathology including intracellular oligomer accumulation, but without extracellular amyloid plaque formation (Tomiya et al., 2010). However, it remains unclear whether A $\beta$  oligomers are accumulated in familial and sporadic AD patient neural cells or not, how intracellular A $\beta$  oligomers play a pathological role, and which compound and/or drugs might rescue the A $\beta$  oligomer-induced pathological phenotypes. Recent developments in iPSC technology have facilitated investigation of phenotypes of patient neural cells *in vitro*, and have helped to overcome the inability to model sporadic AD.

Here we report the derivation and neuronal and astroglial differentiation of iPSCs from a familial AD patient with APP-E693 $\Delta$  mutation as well as a familial case with another APP mutation, and also sporadic cases. Using patient neurons and astrocytes, we addressed the accumulation and possible pathological roles of intracellular A $\beta$  oligomers in

familial and sporadic AD. We found that A $\beta$  oligomers were not proteolytically resistant, and that docosahexaenoic acid (DHA) treatment attenuated cellular phenotypes of AD neural cells with intracellular A $\beta$  oligomers in both sporadic and familial AD patients.

## RESULTS

### iPSC generation and cortical-neuronal differentiation

Dermal fibroblasts were reprogrammed by episomal vectors (Okita et al., 2011). Control hiPSC lines from three unrelated individuals, three and two familial AD hiPSC lines from patients with E693 $\Delta$ [AD(APP-E693 $\Delta$ )] and V717L[AD(APP-V717L)] APP mutations, respectively, and two sporadic hiPSC lines (AD3E211 and AD8K213) from two unrelated patients (Figures S1A) were generated (Figures 1A, 1B and S1B-H). To characterize cortical neurons derived from the hiPSC lines, we established differentiation methods for cortical neurons by a modification of previous procedures (Morizane et al., 2011) (Figure S1I). The differentiated cells expressed the cortical neuron subtype markers SATB2 and TBR1 (Figure 1C), and the differentiated neurons were functionally active (Figures S1J and S1K). There was no prominent difference in differentiation propensity between control and AD neurons (Figures 1D and S1L).

We analyzed the amounts of extra- and intracellular A $\beta$ 40 and A $\beta$ 42 (Figures 1E and 1F). Expectedly, both A $\beta$  species were strongly decreased in all cloned AD(APP-E693 $\Delta$ ) neural cells compared to those in control neural cells. In familial AD(APP-V717L) neural cells, an increase in the extracellular A $\beta$ 42 level and a corresponding decrease in the intracellular A $\beta$ 42 level were observed, and the A $\beta$ 42/A $\beta$ 40 ratio in the culture medium was increased up to 1.5-fold, suggesting that the abnormality of APP metabolism in AD is dependent on the mutation sites in *APP*. Extracellular A $\beta$  levels in sporadic AD neural cells were not changed, compared to that in control neural cells, but intracellular A $\beta$  in sporadic AD8K213 neural cells apparently decreased (that is, below detection limit). APP expression levels in the AD(APP-E693 $\Delta$ ) neural cells were lower than in the others, but the levels of  $\alpha$ - and  $\beta$ -secretase-mediated APP processing remained unaltered in all neural cells (Figures 1G, S1M and S1N). Soluble APP $\beta$  production was strongly inhibited by treatment with

$\beta$ -secretase inhibitor IV (BSI) (Figure 1G). A $\beta$  levels in the original fibroblasts and iPSC-derived astrocytes, in which APP expression levels were relatively higher than in neural cells (data not shown), were lower than those of the corresponding neural cells (Figures S1O and S1P).

Intracellular accumulation of A $\beta$  oligomers in AD(APP-E693 $\Delta$ ) and one of the sporadic AD neural cells

Using an immunocytochemical method with the A $\beta$  oligomer-specific antibody NU1 (Lambert et al., 2007), we investigated whether AD(APP-E693 $\Delta$ ) neural cells harbor A $\beta$  oligomers or not. We found that A $\beta$  oligomers were accumulated as puncta in the neurons of AD(APP-E693 $\Delta$ ) and one of the sporadic AD (Figure 2A). The area of A $\beta$  oligomer-positive puncta was significantly increased in AD(APP-E693 $\Delta$ ) neuronal cells relative to control neuronal cells (Figure 2B). Dot-blot analysis using cell lysates revealed that A $\beta$  oligomers were markedly elevated in the AD(APP-E693 $\Delta$ ) and sporadic AD8K213 neural cells (Figures 2C and 2D), whereas A $\beta$  oligomers were not detected in the culture medium (data not shown). Another antibody against A $\beta$ , 11A1, which detects low-molecular weight oligomers rather than A $\beta$  monomer (Murakami et al., 2010), showed similar results to those observed with NU1 (Figures S2A-S2D). However, A $\beta$  oligomers were not detected in cell lysates from the fibroblasts from which iPSC cell lines were generated (Figure S2E). To confirm whether A $\beta$  oligomers were derived from mutant APP(E693 $\Delta$ ), we transduced a lentiviral vector driven by EF1 $\alpha$  promoter to overexpress wild or mutant APP(E693 $\Delta$ ) in control iPSC-derived neural cells, and found that A $\beta$  oligomers emerged inside the control neural cells (Figure S2F) overexpressing mutant APP(E693 $\Delta$ ).

To investigate intracellular accumulation of A $\beta$  oligomers in astrocytes derived from control and AD iPSC cells, we established an astrocyte-enrichment culture by the method previously reported (Krencik et al., 2011), with modifications (Figures S2G-S2J). Dot-blot analysis using anti-A $\beta$  oligomer antibodies revealed that the astrocytes of AD(APP-E693 $\Delta$ ) and one of the sporadic AD iPSCs accumulated A $\beta$  oligomers intracellularly (Figures 2E,

S2K and S2L), which was compatible with the results of neurons. On the other hand, we detected no difference in uptake of extracellular glutamate between control- and AD astrocytes (Figure S2M).

A $\beta$  oligomers were also detected as a protein band with a molecular mass of 50~60 kDa by western blot analysis (Figures 2F and S2N). The accumulation of A $\beta$  oligomers was inhibited by treatment with BSI (Figures 2A–2G, Figures S2A-S2D and S2N). To clarify whether the E693 $\Delta$  mutation results in accelerated A $\beta$  oligomerization and/or in a proteolytically resistant and stable form of A $\beta$  oligomers, we analyzed the levels of A $\beta$  oligomers over a course of time after BSI treatment. Intracellular A $\beta$  oligomers started to disappear from 2 h after the treatment with BSI reaching almost the control level by 8 h (Figures 2G and 2H). Secretion of A $\beta$ 40 from control neural cells was already inhibited at 2 h after BSI treatment, but that from AD neural cells was under the detection limit in both the presence and absence of BSI (Figure 2I).

Cellular stress responses caused by intracellular A $\beta$  oligomers in AD iPSC-derived neural cells

Extracellular A $\beta$  deposition in patient brains carrying APP with E693 $\Delta$  mutation is predicted to be extremely low, as amyloid PET imaging with a [<sup>11</sup>C] Pittsburgh compound-B (PIB) probe revealed a far lower signal in the patients than those observed in sporadic AD brains (Tomiya et al., 2008). Given that processing by  $\beta$ - and  $\gamma$ -secretases largely proceeds within vesicular endosomal compartments, it was possible that A $\beta$  oligomers were associated with specific organelles. We characterized the A $\beta$  oligomer-positive punctate structures in AD(APP-E693 $\Delta$ ) neural cells and astrocytes by co-immunostaining with antibodies for markers of vesicular compartments and subcellular organelles. Subpopulations of A $\beta$  oligomer-positive puncta in the AD neurons showed positive immunostaining for an ER marker, binding immunoglobulin protein (BiP), an early endosomal marker, early endosome-associated antigen-1 (EEA1), and a lysosomal marker, lysosomal associated marker protein-2 (LAMP2) (data not shown). Puncta were also observed in astrocytes from AD-iPSCs (Figure 2E).

To uncover molecules that might be implicated in the dysfunction of AD(APP-E693Δ) neural cells, we analyzed gene expression profiles of control and the AD neural cells (Figure 3A and Table S1). Gene ontology analysis revealed that oxidative stress-related categories including peroxiredoxin, oxidoreductase, and peroxidase activities were up-regulated in the AD, whereas glycosylation-related categories were down-regulated (Figure 3B, 3C and Table S1), suggesting that ER and Golgi function might be perturbed in the AD neural cells. Western blot analysis clarified that the amounts of BiP were elevated in the neurons and astrocytes of the AD(APP-E693D) case and of one of the sporadic AD cases, AD8K21, but not in fibroblasts (Figures 3D, S3A-S3F). We also found that BSI treatment prevented not only the increase of A $\beta$  oligomer-positive puncta area per cell in the context of AD(APP-E693Δ) lines but also decreased the amount of BiP and cleaved caspase-4 (Figures 3D-3F). The antioxidant gene peroxiredoxin-4 was the most highly upregulated gene (Figure 3C). Western blot analysis confirmed that the amount of peroxiredoxin-4 was increased up to approximately 5- to 7-fold in lysates from AD(APP-E693Δ) and one of the sporadic AD, AD8K213 neural cells, but not fibroblasts, and was decreased by the BSI treatment (Figures 3D, 3G, S3A, S3D, S3G, and S3H), indicating that anti-oxidant stress response was provoked by A $\beta$  oligomer formation in AD(APP-E693Δ) and sporadic AD8K213. To identify pathogenic species evoking oxidative stress in AD(APP-E693Δ), we visualized reactive oxygen species (ROS) and found that ROS was increased in both neurons and astrocytes in AD(APP-E693Δ) and AD8K213 (Figures 3H-3J, Figures S3I –S3L). This increase was counteracted by the BSI treatment. These results indicated that intracellular A $\beta$  oligomers provoked both ER- and oxidative stress with the increase in ROS probably via a vicious cycle between ER- and oxidative stress (Malhotra and Kaufman, 2007).

#### Alleviation of intracellular A $\beta$ oligomer-induced cellular stress by DHA

We evaluated BSI and three additional drugs that had been reported to improve ER stress or to inhibit ROS generation: 1) DHA (Begum et al., 2012), 2) dibenzoylmethane (DBM14-26) (Takano et al., 2007) and 3) NSC23766 (Lee et al., 2002) (Figures 4 and S6).

DHA treatment significantly decreased the protein level of BiP, cleaved caspase-4, and peroxiredoxin-4 in AD (APP-E693 $\Delta$ ) neural cells (Figures 4A, 4B, S4A, and S4B), and BiP and peroxiredoxin-4 in sporadic AD8K213 (Figures S4C and S4D). Furthermore, DHA treatment also decreased the generation of ROS in AD(APP-E693 $\Delta$ ) neural cells (Figures 4C and 4D), while the amount of A $\beta$  oligomers in cell lysates was not altered (Figures S4E-S4G). By contrast, either high-concentration of DHA, DBM14-26, or NSC23766 treatment increased the protein level of BiP (Figure S4B). Finally, to confirm the protective effects of DHA in short-term screening, we analyzed the effect on the survival of AD(APP-E693 $\Delta$ ) neural cells in a long-term culture period. Neuronal cells were labeled with a lentiviral vector expressing synapsin I-promoter-driven EGFP and cultivated in the medium depleted of neurotrophic factors and neural culture supplements mix. The real-time survival rate of AD(APP-E693 $\Delta$ ) neurons was lower than that of normal control neurons, however, DHA treatment for 16 days partially rescued AD(APP-E693 $\Delta$ ) cell viability (Figure 4E-4G). However, that of sporadic AD(AD3E211, AD8K213) neurons for 16 days was unchanged (Figure 4E, 4F, and Table S2). We confirmed these results by LDH assay (Figure 4G). The AD(APP-E693 $\Delta$ ) neurons were also vulnerable to oxidative stress by hydrogen peroxide treatment (Figure S4H). Extracellular A $\beta$  levels were not altered in the assay (Figure 4H).

## DISCUSSION

The present study showed that neural cells derived from a patient carrying the pathogenic APP-E693 $\Delta$  mutation and one sporadic AD patient produce intracellular A $\beta$  oligomers, and the use of these neural cells provided an experimental system for addressing whether such oligomers would cause cellular stress and the killing of neurons, and how such intracellular A $\beta$  oligomers might contribute to the disease pathogenesis, despite only one patient carrying the E693 $\Delta$  mutation being available. Our findings also suggest that the possible heterogeneity of familial and sporadic AD stemmed from phenotypic differences of intracellular A $\beta$  oligomers, and suggested the possibility that DHA, a drug that failed in some clinical trials of AD treatment, might be effective in a portion of AD patients.

We demonstrated that A $\beta$  oligomers were formed and accumulated inside

AD(APP-E693 $\Delta$ ) and sporadic AD(AD8K213) neurons by immunostaining (Figures 2A and 2B), dot blot analysis (Figures 2C and 2D), and western blot analysis (Figures 2F and S2N). In addition, intracellular accumulation of A $\beta$  oligomers, which have been supposed to be proteolytically resistant, disappeared after treatment with BSI in both AD neurons (Figures 2G and 2H), indicating that AD(APP-E693 $\Delta$ ) and sporadic AD(AD8K213) neurons still seemed to retain a degrading activity towards A $\beta$  oligomers in which proteasomes, autophagosomes and/or lysosomes may be involved, and thereby that the pathological property of A $\beta$  oligomers in a part of AD might be completely abrogated. The sporadic AD(AD8K213) neurons may retain a specific cellular environment that permits the formation of A $\beta$  oligomers. Further studies to identify factors causing such an environment are needed.

We observed that accumulation of A $\beta$  oligomers induced ER stress and oxidative stress both in AD(APP-E693 $\Delta$ ) and in sporadic AD(AD8K213) neurons, although caspase-4 activation appeared not to accompany sporadic AD, probably due to the lesser extent of ER stress compared to AD(APP-E693 $\Delta$ ). Previously, Nishitsuji et al. (2009) reported that accumulated A $\beta$  oligomers in ER provoke ER stress. This result suggests that oligomers represent a self-aggregating state of A $\beta$ , and during this process A $\beta$  generates ROS, which is supported by the fact that A $\beta$  coordinates the metal ions Zn, Fe and Cu, which induce oligomerization of A $\beta$ . Iron and copper then cause the generation of toxic ROS and calcium dysregulation (Barnham et al., 2004), leading to membrane lipid peroxidation and impairment of the function of a range of membrane-associated proteins (Hensley et al., 1994; Butterfield, 2003), with anti-oxidant factors being thought to protect ER-stress-induced cellular toxicities (Malhotra and Kaufman, 2007).

We found that intracellular A $\beta$  oligomers were accumulated not only in a case of familial AD with APP-E693 $\Delta$  mutation but also in a sporadic AD case, although only three clones derived from one familial AD patient carrying APP-E693 $\Delta$  mutation and two clones from two sporadic AD patients were analyzed in this study due to the limited number of patients. In contrast, in familial AD with APP-V717L mutation, also only one case, intracellular A $\beta$  oligomers were not detected, but the extracellular A $\beta$ 42/A $\beta$ 40 ratio, which is increased in mutant presenilin-mediated familial AD as reported previously (Yagi et al.,

2011), was increased, lending support to the notion that AD could be classified into two categories, such as intracellular A $\beta$ -type and extracellular A $\beta$ -type. Although it has been supposed that environmental factors and/or the aging process contribute to neurodegenerative diseases, our finding supports the idea that a genetic factor might play a role in a part of sporadic AD, compatible with a previous report (Israel et al., 2012). However, it will require a larger sample size to identify the genetic factor. The sporadic AD case with intracellular A $\beta$  oligomers might correspond to the case without extracellular A $\beta$ 40 elevation of Israel et al. (2012). Analysis of neurons and astrocytes, as we performed here, from larger numbers of patients might result in the classification of sporadic AD.

To date, the clinical effectiveness of DHA treatment is still controversial (Freund-Levi et al., 2006; Quinn et al., 2010). It is of particular interest that one of two sporadic AD neurons accumulated intracellular A $\beta$  oligomers and showed cellular phenotypes that could respond to DHA, but the other did not, and this result may explain why DHA treatment was effective for a part of AD patients, the intracellular A $\beta$  oligomer-associated type of AD, although the timing, that is, the stage of disease development, for starting the treatment would be another critical factor. These results may suggest that patient-specific iPSCs provides a chance to re-evaluate the effect of a dropped-off drug in AD clinical trials, depending on selection of the type of patient. In the present study, the amount of A $\beta$  oligomers in our culture was not affected by DHA, although it would be effective for reducing cellular stresses, and reducing oligomerization of A $\beta$  was also presumed to be a candidate mechanism of DHA treatment (Cole and Frautschy, 2006). These results indicate that therapy with DHA would be one of symptom-alleviation. Furthermore, the data showing that BSI treatment leads to a reduction in ROS formation at a relatively similar level (Figure 2G) both in both AD and control cells might indicate an A $\beta$  oligomer-independent effect, in addition to an A $\beta$  oligomer-dependent effect of BSI.

In any event, patient-specific iPSCs would provide the disease pathogenesis irrespective of the disease being in familial or sporadic form, as well as enable evaluation of a drug and patient classification of AD.

## **FIGURE LEGENDS**

**Figure 1, see also Figure S1. Establishment of control and AD patient-specific iPSCs, and derivation of cortical neurons producing A $\beta$ s from iPSCs.**

(A) Established iPSCs, from both controls and AD patients, showed embryonic stem cell-like morphology (Phase) and expressed pluripotent stem cell markers, NANOG (Red) and TRA1-60 (Green). Scale bar: 200  $\mu$ m. (B) Genomic DNA sequences showed the presence of the homozygous genotype for E693 deletion and the heterozygous genotype for V717L mutation on *APP* gene only in AD iPSCs. (C) Estimation of neuronal differentiation from control and AD-iPSCs. After 2 months of differentiation, neurons were immunostained with antibodies against neuronal marker TUJ1, and cortical neuron markers TBR1 and SATB2. Scale bar: 100  $\mu$ m. (D) Proportions of TUJ1, TBR1, SATB2-positive cells in control and AD-iPSCs. Data represent mean  $\pm$  S.D. (n = 3 per clone). (E) A $\beta$ 40 and A $\beta$ 42 secreted from hiPSC-derived neural cells into medium (extracellular A $\beta$ ) were measured by sandwich ELISA at 48 h after the last medium change. Data represent mean  $\pm$  S.D. (n = 3 per clone). Levels of A $\beta$ 40 and A $\beta$ 42 in AD(APP-E693 $\Delta$ ) without  $\beta$ -secretase inhibitor IV (BSI, 1  $\mu$ M) were significantly lower than those of the others (\**p* < 0.006), and the level of A $\beta$ 42 and the ratio of A $\beta$ 42/A $\beta$ 40 in AD(APP-V717L) without BSI were significantly higher than those of the others (\**p* < 0.001). There are significant differences between DMSO (control) and BSI treatment in each case (\**p* < 0.001) except that of AD(APP-E693 $\Delta$ ) for A $\beta$ 42. (F) A $\beta$ 40 and A $\beta$ 42 in cell lysates (intracellular A $\beta$ ). N.D., not detected. Data represent mean  $\pm$  S.D. (n = 3 per clone). (G) Amount of soluble APP $\beta$  was not altered in control and AD. Data represent mean  $\pm$  SD (n = 3 per clone).

**Figure 2, see also Figure S2. Familial AD(APP-E693 $\Delta$ ) and a sporadic AD iPSC-derived neurons have intracellular A $\beta$  oligomers.**

(A) Intracellular A $\beta$  oligomer accumulation in iPSC-derived neurons (Red, MAP2- positive cells) was detected by anti-A $\beta$  oligomer monoclonal antibody NU1 (Green) with a punctate pattern. A $\beta$  oligomer accumulation was massive in AD(APP-E693 $\Delta$ ) and sporadic AD(AD8K213) neurons, but only faint in control neurons. Treatment with 1  $\mu$ M BSI decreased the A $\beta$  oligomer accumulation. DAPI, nuclear staining (Blue). Scale bar: 30  $\mu$ m. (B) Quantification of A $\beta$  oligomer accumulation in panel A; ratio of the NU1-positive area

in the MAP2-positive area was analyzed. Data represent mean  $\pm$  S.D. ( $n = 3$  per clone). A $\beta$  oligomer levels in the AD(APP-E693 $\Delta$ ) and sporadic AD(AD8K213) neural cells without BSI were significantly different from those of other neural cells ( $*p < 0.005$ ) and from corresponding neural cells with BSI ( $\#p < 0.005$ ). (C) Dot-blot analysis using NU1 antibody. Control (N116213, N117322, 409B2), APP-E693 $\Delta$ (APP1E111, APP1E211, APP1E211), APP-V717L (APP2E22, APP2E26), sporadic AD (AD3E211, AD8K213) neural cells were dotted from the left. Blank is RIPA buffer only. (D) Signals of blots in panel C were quantified. Data represent mean  $\pm$  S.D. ( $n = 3$  per clone). A $\beta$  oligomer levels in AD(APP-E693 $\Delta$ ) and sporadic AD(AD8K213) neurons without BSI were significantly different from those of other neurons ( $*p < 0.001$ ) and from corresponding neurons treated with 1  $\mu$ M BSI ( $\#p < 0.001$ ). (E) A $\beta$  oligomer accumulation in AD astrocytes. (F) Western blot analysis of control and AD neural cells in the presence or absence of BSI. 6E10-positive  $\approx$ 55 kDa protein bands in cell lysates of AD(APP-E693 $\Delta$ ) and sporadic AD(AD8K213) neural cells disappeared by BSI treatment (1  $\mu$ M). (G) Disappearance of A $\beta$  oligomers after BSI treatment was analyzed by dot-blot analysis using NU1 antibody. Intracellular A $\beta$  oligomers started to disappear from 2 h after BSI treatment. (H) Signals of blots in panel G were quantified. Data represent mean  $\pm$  S.D. ( $n = 3$  per clone). BSI treatment (1  $\mu$ M) decreased intracellular A $\beta$  in AD neural cells was reduced to 16~23% of vehicle control by 8 h. *Post hoc* analysis revealed that the amounts of A $\beta$  oligomers at 2 h after BSI treatment were significantly decreased compared to those of DMSO (control) ( $*p < 0.005$ ). (I) Changes in extracellular A $\beta$ 40 levels were analyzed in the experimental condition of panel G. Data represent mean  $\pm$  SD ( $n = 3$  per clone).

**Figure 3, see also Figure S3 and Table S1. Cellular stress responses caused by intracellular A $\beta$  oligomers in familial AD(APP-E693 $\Delta$ ) and sporadic AD(AD8K213) iPSC-derived neural cells.**

(A) Hierarchical clustering analysis of differentiated neuronal cells, and heatmap of significantly up- and down-regulated genes in AD neural cells. Statistically significant cut-off p-value is  $<0.05$ . (B) GO term list, calculated from the significantly altered gene expression patterns in microarray analysis of AD versus control neural cells. (C) Altered

expression levels of genes related to peroxidation activity detected by GO analysis. All values were significantly different from that of control ( $p < 0.05$ ). (D) Western blot analysis of ER stress markers (BiP and caspase-4), peroxiredoxin-4 and a reference protein ( $\beta$ -actin) in the presence or absence of BSI. (E-G) Densitometric analysis of panel D. Measured values of proteins were normalized by that of  $\beta$ -actin. Data represent mean  $\pm$  SD ( $n = 3$  per clone). Levels of BiP (E), cleaved caspase-4 (F) and peroxiredoxin-4 (G) in AD(APP-E693 $\Delta$ ) and sporadic AD(AD8K213) neural cells without BSI were significantly different from those of the other neural cells (\*\* $p < 0.005$ ). (H) Typical images of ROS staining, detected by HPF or CellROX, in control and AD neural cells with or without BSI treatment. Scale bars: 30  $\mu$ m. (I,J) Quantitative data of panel H, ROS-HPF (I) and ROS-CellROX (J). Each value was shown as a ratio of the HPF-stained or CellROX area (average of random 25 fields per sample), adjusted with DAPI counts. Data represent mean  $\pm$  SD ( $n = 3$  per clone). ROS-generation levels in AD(APP-E693 $\Delta$ ) and sporadic AD(AD8K213) neural cells were significantly different from those of the others (\*\* $p < 0.001$ ). Data represent mean  $\pm$  SD ( $n = 3$  per clone).

**Figure 4, see also Figure S4 and Table S2. DHA alleviated cellular stress caused by intracellular A $\beta$  oligomers.**

(A) Control and AD(APP-E693 $\Delta$ ) neural cells at day 72 were treated with DHA for 48 h. Then, cells were lysed and subjected to immunoblot analysis (DHA concentrations: 1, 5 and 15  $\mu$ M). (B) Densitometric analysis of panel A. Measured values were normalized by that of  $\beta$ -actin. Data represent mean  $\pm$  SD ( $n = 3$  per clone). Two-way ANOVA showed significant main effects of DHA treatment (BiP,  $F_{(3,64)} = 136.712$ ,  $p < 0.001$ ; cleaved caspase-4,  $F_{(3,64)} = 50.855$ ,  $p < 0.001$ ) with a significant interaction between APP mutation and DHA treatment (BiP,  $F_{(3,64)} = 99.658$ ,  $p < 0.001$ ; cleaved caspase-4,  $F_{(3,64)} = 53.005$ ,  $p < 0.001$ ). *Post hoc* analysis revealed significant differences between DMSO (control) and DHA treatment (1, 5 and 15  $\mu$ M) in AD(APP-E693 $\Delta$ ) neural cells (\*\* $p < 0.001$ ). Two-way ANOVA for peroxiredoxin-4 showed significant main effects of DHA treatment ( $F_{(3,64)} = 16.995$ ;  $p < 0.001$ ) with a significant interaction between APP mutation and DHA treatment ( $F_{(3,64)} = 32.093$ ;  $p < 0.001$ ). *Post hoc* analysis revealed significant differences

between DMSO (control) and DHA treatment (5 and 15  $\mu$ M) in AD(APP-E693 $\Delta$ ) neural cells (\*\* $p < 0.001$ ). In control neural cells, 5  $\mu$ M DHA group was significantly different from the other groups (\* $p < 0.005$ ). (C) Typical images of ROS-CellROX and Hoechst33342 signals after treatment with vehicle or 5  $\mu$ M DHA. Scale bar: 50  $\mu$ m. (D) Quantitative data of panel C. Each value indicated the ratio of CellROX-stained area (average of random 25 fields per sample), adjusted with DAPI counts. Data represent mean  $\pm$  SD (n = 3 per clone). Two-way ANOVA showed significant main effects of DHA treatment ( $F_{(1,32)} = 43.140$ ;  $p < 0.001$ ) with a significant interaction between the APP mutation and DHA treatment ( $F_{(3,32)} = 23.410$ ;  $p < 0.001$ ). The DHA group in AD(APP-E693 $\Delta$ ) neural cells was significantly different from the other groups (\* $p < 0.005$ ). (E) Real-time survival rate of control and AD neural cells without and with DHA showing cell viability. The numbers of control and AD(APP-E693 $\Delta$ ) neurons with Synapsin I promoter-driven EGFP were sequentially imaged (average of 25 random fields per sample) and counted to assess survival ratio (n=3 per clone). Data represent mean  $\pm$  SD (n = 3 per clone). In the cell survival ratio, three-way ANOVA showed significant main effects of the APP mutation ( $F_{(1,256)} = 377.611$ ;  $p < 0.001$ ), DHA treatment ( $F_{(1,256)} = 36.117$ ;  $p < 0.001$ ) and time ( $F_{(7,256)} = 65.272$ ;  $p < 0.001$ ), with significant interactions between the APP mutation and DHA treatment ( $F_{(1,256)} = 18.315$ ;  $p < 0.001$ ), between the APP mutation and time ( $F_{(7,256)} = 20.023$ ;  $p < 0.001$ ), between DHA treatment and time ( $F_{(7,256)} = 4.534$ ;  $p < 0.001$ ), and among all three factors ( $F_{(7,256)} = 5.277$ ;  $p < 0.001$ ). *Post hoc* analysis revealed that, on days 14 and 16, AD(APP-E693 $\Delta$ ) neural cells were more vulnerable in the long culture than control neural cells, and DHA treatment rescued the vulnerability (\* $p < 0.001$ ). (F) Typical images of Synapsin::EGFP neurons used in real-time survival assay. Scale bar: 50  $\mu$ m (G) Cytotoxicity in neural culture derived from control and AD iPSCs after treatment with DHA (5  $\mu$ M) for 16 days. Measured fluorescent LDH release served as a measure of cytotoxicity. Data represent mean  $\pm$  SD (n = 3 per clone). Two-way ANOVA showed significant main effects of DHA treatment ( $F_{(1,32)} = 16.710$ ;  $p < 0.001$ ) with a significant interaction between APP-E693 $\Delta$  mutation and DHA treatment ( $F_{(3,32)} = 9.210$ ;  $p < 0.005$ ). There was a significant difference in AD(APP-E693 $\Delta$ ) neural cells between the DMSO (control) and DHA groups (\* $p < 0.05$ ). (H) A $\beta$ 40 and A $\beta$ 42 secreted from

hiPSC-derived neurons into medium (extracellular A $\beta$ ) at day 16 of the long-term culture were measured by MSD electrochemiluminescence assay at 48 h after the last medium change. Data represent mean  $\pm$  SD (n = 3 per clone).

## **EXPERIMENTAL PROCEDURES**

### Derivation of patient-specific fibroblasts

Control and AD-derived human dermal fibroblasts (HDF) were generated from explants of 3-mm dermal biopsies. After 1-2 weeks, fibroblast outgrowths from the explants were passaged.

### iPSC generation

Human cDNAs for reprogramming factors were transduced in HDF with episomal vectors (*SOX2*, *KLF4*, *OCT4*, *L-MYC*, *LIN28*, siRNA for p53). Several days after transduction, fibroblasts were harvested and replated on an SNL feeder cell layer. On the following day, the medium was changed to primate embryonic stem cell medium (ReproCELL Inc., Japan) supplemented with 4 ng/ml basic FGF (Wako Pure Chemicals Industries, Ltd, Japan). The medium was changed every other day. Thirty days after transduction, iPSC colonies were picked up.

### Statistical analysis

All data are shown as mean  $\pm$  S.D. For comparisons of the mean between two groups, statistical analysis was performed by applying Student's *t* tests after confirming equality between the variances of the groups. If the variances were unequal, Mann-Whitney *U*-tests were performed (SigmaPlot software, ver.11.2; Systat Software Inc.). Comparisons of the mean among three groups or more were done by one-way, two-way, or three-way analysis of variance (ANOVA) followed by *post-hoc* test using Student-Newman-Keuls Method (SigmaPlot software). *P* values < 0.05 were considered significant.

## **ACCESSION NUMBERS**

The Gene Expression Omnibus accession number for microarray data reported in this paper

is GSE43326 (gene-expression comparison between control and AD clones), GSE43382 (gene-expression change along with the astroglial differentiation), and GSE43328 (gene-expression comparison of generated iPS cells).

## **ACKNOWLEDGEMENTS**

We would like to express our sincere gratitude to all our coworkers and collaborators, Mari Ohnuki, Megumi Kumazaki, Mitsuyo Kawada, Fumihiko Adachi, Takako Enami and Misato Funayama for technical assistance, Nobuya Inagaki and Norio Harada for technical advice, and Kazumi Murai for editing the manuscript. This research was funded in part by a grant from the Funding Program for World-Leading Innovative R&D on Science and Technology (FIRST Program) of the Japan Society for the Promotion of Science (JSPS) (SY), from the Alzheimer's Association (IIRG-09-132098) (HM), from the JST Yamanaka iPS cell special project (SY, HI), from CREST (HI, HM, NI, TT), from a Grant-in-Aid from the Ministry of Health, Labour and Welfare of Japan (HI), from a Grant-in-Aid for Scientific Research on Innovative Area “Foundation of Synapse and Neurocircuit Pathology” (22110007) from the Ministry of Education, Culture, Sports, Science and Technology of Japan (HI, NI), and from the Japan Research Foundation for Clinical Pharmacology (HI). The experimental protocol dealing with human or animal subjects were approved by the institutional review board at each institute. HI conceived the project; TK, NI, MA, and HI designed the experiments; TK, NI, MA, KW, CK, RN, NE, NY and KT sukita performed the experiments; TK, NI, MA, and HI analyzed the data; KO, IA, KM, TN, KI, WLK, OH, SH, TC contributed reagents, materials and analysis tools; YK, YO, YS, MN, KY, SY, SS, TA, RH and SU recruited the patients; RT, HM and SY provided critical reading and scientific discussions; TS, KK, TT and KTakahashi performed microarray analysis; TA performed karyotyping; AW performed Bisulfite Genomic Sequencing; KI and DW performed electrophysiology; KT sukita, TK and HH produced lentivirus; HI, NI, MA, and TK wrote the paper.

## **DISCLOSURE OF POTENTIAL CONFLICTS OF INTEREST**

S.Y. is a member without salary of the scientific advisory boards of iPierian, iPS Academia

Japan, Megakaryon Corporation, and Retina Institute Japan.

## REFERENCES

Barnham, K.J., Masters, C.L., Bush, A.I. (2004). Neurodegenerative diseases and oxidative stress. *Nat Rev Drug Discov* 3, 205-214.

Begum, G., Kintner, D., Liu, Y., Cramer, S.W., Sun, D. (2012). DHA inhibits ER Ca<sup>2+</sup> release and ER stress in astrocytes following in vitro ischemia. *J Neurochem* 120, 622-630.

Butterfield DA. (2003). Amyloid  $\beta$ -peptide [1-42]-associated free radical-induced oxidative stress and neurodegeneration in Alzheimer's disease brain: mechanisms and consequences. *Curr Med Chem* 10, 2651-2659.

Cole, G.M., Frautschy, S.A. (2006). Docosahexaenoic acid protects from amyloid and dendritic pathologies in an Alzheimer's disease mouse model. *Nutr Health* 18, 249-259.

Freund-Levi, Y., Eriksdotter-Jönhagen, M., Cederholm, T., Basun, H., Faxén-Irving, G., Garlind, A., Vedin, I., Vessby, B., Wahlund, L.O., Palmblad, J. (2006). Omega-3 fatty acid treatment in 174 patients with mild to moderate Alzheimer disease: OmegAD study: a randomized double-blind trial. *Arch Neurol* 63, 1402-1408.

Gong, Y., Chang, L., Viola, K.L., Lacor, P.N., Lambert, M.P., Finch, C.E., Krafft, G.A., and Klein, W.L. (2003). Alzheimer's disease-affected brain: presence of oligomeric A $\beta$  ligands (ADDLs) suggests a molecular basis for reversible memory loss. *Proc Natl Acad Sci USA* 100, 10417-10422.

Haass, C., Selkoe, D.J. (2007). Soluble protein oligomers in neurodegeneration: lessons from the Alzheimer's amyloid  $\beta$ -peptide. *Nat Rev Mol Cell Biol* 8, 101-112.

Hensley K, Carney JM, Mattson MP, Aksenova M, Harris M, Wu JF, Floyd RA, Butterfield

DA. (1994). A model for  $\beta$ -amyloid aggregation and neurotoxicity based on free radical generation by the peptide: relevance to Alzheimer disease. *Proc Natl Acad Sci USA* *91*, 3270-3274.

Israel, M.A., Yuan, S.H., Bardy, C., Reyna, S.M., Mu, Y., Herrera, C., Hefferan, M.P., Van Gorp, S., Nazor, K.L., Boscolo, F.S., *et al.* (2012). Probing sporadic and familial Alzheimer's disease using induced pluripotent stem cells. *Nature* *482*, 216-220.

Kassler, K., Horn, A.H., Sticht, H. (2010). Effect of pathogenic mutations on the structure and dynamics of Alzheimer's A $\beta$ 42-amyloid oligomers. *J Mol Model* *16*, 1011-1020.

Krafft, G.A., Klein, W.L. (2010). ADDLs and the signaling web that leads to Alzheimer's disease. *Neuropharmacology* *59*: 230-242.

Krencik, R., Weick, J.P., Liu, Y., Zhang, Z.J., and Zhang, S.C. (2011). Specification of transplantable astroglial subtypes from human pluripotent stem cells. *Nat Biotechnol* *29*, 528-534.

Kuo, Y.M., Emmerling, M.R., Vigo-Pelfrey, C., Kasunic, T.C., Kirkpatrick, J.B., Murdoch, G.H., Ball, M.J., Roher, A.E. (1996). Water-soluble A $\beta$ (N-40, N-42) oligomers in normal and Alzheimer disease brains. *J Biol Chem* *271*: 4077-4081.

Lambert, M.P., Velasco, P.T., Chang, L., Viola, K.L., Fernandez, S., Lacor, P.N., Khuon, D., Gong, Y., Bigio, E.H., Shaw, P., *et al.* (2007). Monoclonal antibodies that target pathological assemblies of A $\beta$ . *J Neurochem* *100*, 23-35.

Lee, M., You, H.J., Cho, S.H., Woo, C.H., Yoo, M.H., Joe, E.H., Kim, J.H. (2002). Implication of the small GTPase Rac1 in the generation of reactive oxygen species in response to  $\beta$ -amyloid in C6 astrogloma cells. *Biochem J* *366*, 937-943.

Lesné, S., Koh, M.T., Kotilinek, L., Kaye, R., Glabe, C.G., Yang, A., Gallagher, M., Ashe, K.H. (2006). A specific amyloid- $\beta$  protein assembly in the brain impairs memory. *Nature* 440, 352-357

Malhotra, J.D., Kaufman, R.J. (2007). Endoplasmic reticulum stress and oxidative stress: a vicious cycle or a double-edged sword? *Antioxid Redox Signal* 9, 2277-2293.

Morizane, A., Doi, D., Kikuchi, T., Nishimura, K., and Takahashi, J. (2011). Small-molecule inhibitors of bone morphogenic protein and activin/nodal signals promote highly efficient neural induction from human pluripotent stem cells. *J Neurosci Res* 89, 117-126.

Murakami, K., Horikoshi-Sakuraba, Y., Murata, N., Noda, Y., Masuda, Y., Kinoshita, N., Hatsuta, H., Murayama, S., Shirasawa, T., Shimizu, T., *et al.* (2010). Monoclonal antibody against the turn of the 42-residue amyloid  $\beta$ -protein at positions 22 and 23. *ACS Chemical Neuroscience* 1, 747-756.

Nishitsuji, K., Tomiyama, T., Ishibashi, K., Ito, K., Teraoka, R., Lambert, M.P., Klein, W.L., Mori, H. (2009). The E693 $\Delta$  mutation in amyloid precursor protein increases intracellular accumulation of amyloid  $\beta$  oligomers and causes endoplasmic reticulum stress-induced apoptosis in cultured cells. *Am J Pathol* 174, 957-969.

Noguchi, A., Matsumura, S., Dezawa, M., Tada, M., Yanazawa, M., Ito, A., Akioka, M., Kikuchi, S., Sato, M., Ideno, S., *et al.* (2009) Isolation and characterization of patient-derived, toxic, high mass amyloid  $\beta$ -protein (A $\beta$ ) assembly from Alzheimer disease brains. *J Biol Chem* 284, 32895-32905.

Okita, K., Matsumura, Y., Sato, Y., Okada, A., Morizane, A., Okamoto, S., Hong, H., Nakagawa, M., Tanabe, K., Tezuka, K., *et al.* (2011). A more efficient method to generate integration-free human iPS cells. *Nat Methods* 8, 409-412.

Quinn, J.F., Raman, R., Thomas, R.G., Yurko-Mauro, K., Nelson, E.B., Van Dyck, C., Galvin, J.E., Emond, J., Jack, C.R., Jr., Weiner, M., *et al.* (2010). Docosahexaenoic acid supplementation and cognitive decline in Alzheimer disease: a randomized trial. *JAMA* *304*, 1903-1911.

Shankar, G.M., Li, S., Mehta, T.H., Garcia-Munoz, A., Shepardson, N.E., Smith, I., Brett, F.M., Farrell, M.A., Rowan, M.J., Lemere, C.A., *et al.* (2008). Amyloid- $\beta$  protein dimers isolated directly from Alzheimer's brains impair synaptic plasticity and memory. *Nat Med* *14*, 837-842.

Shimada, H., Ataka, S., Tomiyama, T., Takechi, H., Mori, H., Miki, T. (2011). Clinical course of patients with familial early-onset Alzheimer's disease potentially lacking senile plaques bearing the E693 $\Delta$  mutation in amyloid precursor protein. *Dement Geriatr Cogn Disord* *32*, 45-54.

Takano, K., Kitao, Y., Tabata, Y., Miura, H., Sato, K., Takuma, K., Yamada, K., Hibino, S., Choshi, T., Iinuma, M., *et al.* (2007). A dibenzoylmethane derivative protects dopaminergic neurons against both oxidative stress and endoplasmic reticulum stress. *Am J Physiol Cell Physiol* *293*, C1884-1894.

Tomiyama, T., Matsuyama, S., Iso, H., Umeda, T., Takuma, H., Ohnishi, K., Ishibashi, K., Teraoka, R., Sakama, N., Yamashita, T., *et al.* (2010). A mouse model of amyloid  $\beta$  oligomers: their contribution to synaptic alteration, abnormal tau phosphorylation, glial activation, and neuronal loss *in vivo*. *J Neurosci* *30*, 4845-4856.

Tomiyama, T., Nagata, T., Shimada, H., Teraoka, R., Fukushima, A., Kanemitsu, H., Takuma, H., Kuwano, R., Imagawa, M., Ataka, S., *et al.* (2008). A new amyloid  $\beta$  variant favoring oligomerization in Alzheimer's-type dementia. *Ann Neurol* *63*, 377-387.

Walsh, D.M., Klyubin, I., Fadeeva, J.V., Cullen, W.K., Anwyl, R., Wolfe, M.S., Rowan, M.J., and Selkoe, D.J. (2002). Naturally secreted oligomers of amyloid  $\beta$  protein potently inhibit hippocampal long-term potentiation *in vivo*. *Nature* *416*, 535-539.

Yagi, T., Ito, D., Okada, Y., Akamatsu, W., Nihei, Y., Yoshizaki, T., Yamanaka, S., Okano, H., Suzuki, N. (2011). Modeling familial Alzheimer's disease with induced pluripotent stem cells. *Hum Mol Genet* *20*, 4530-4539.

Figure 1

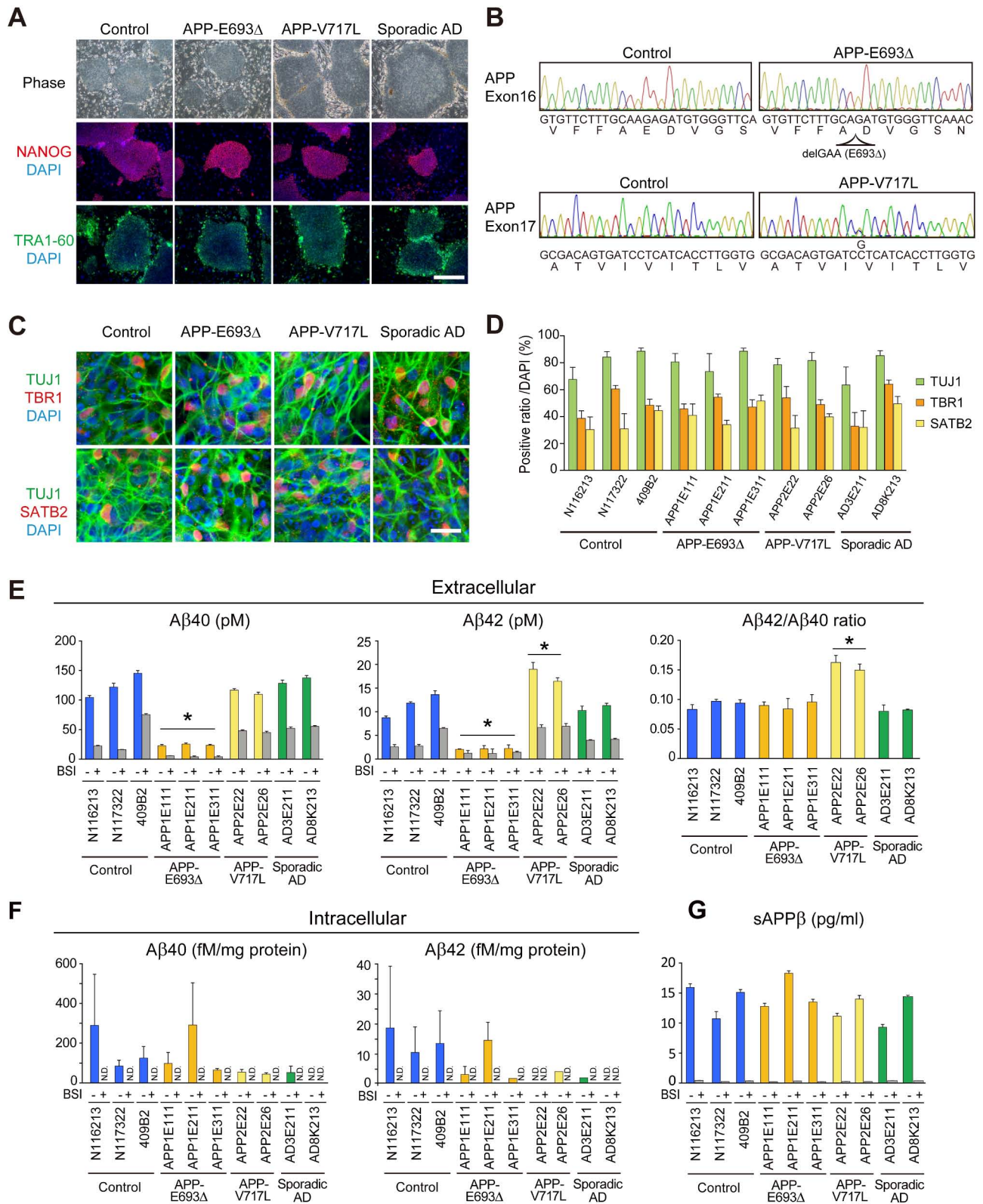


Figure 2

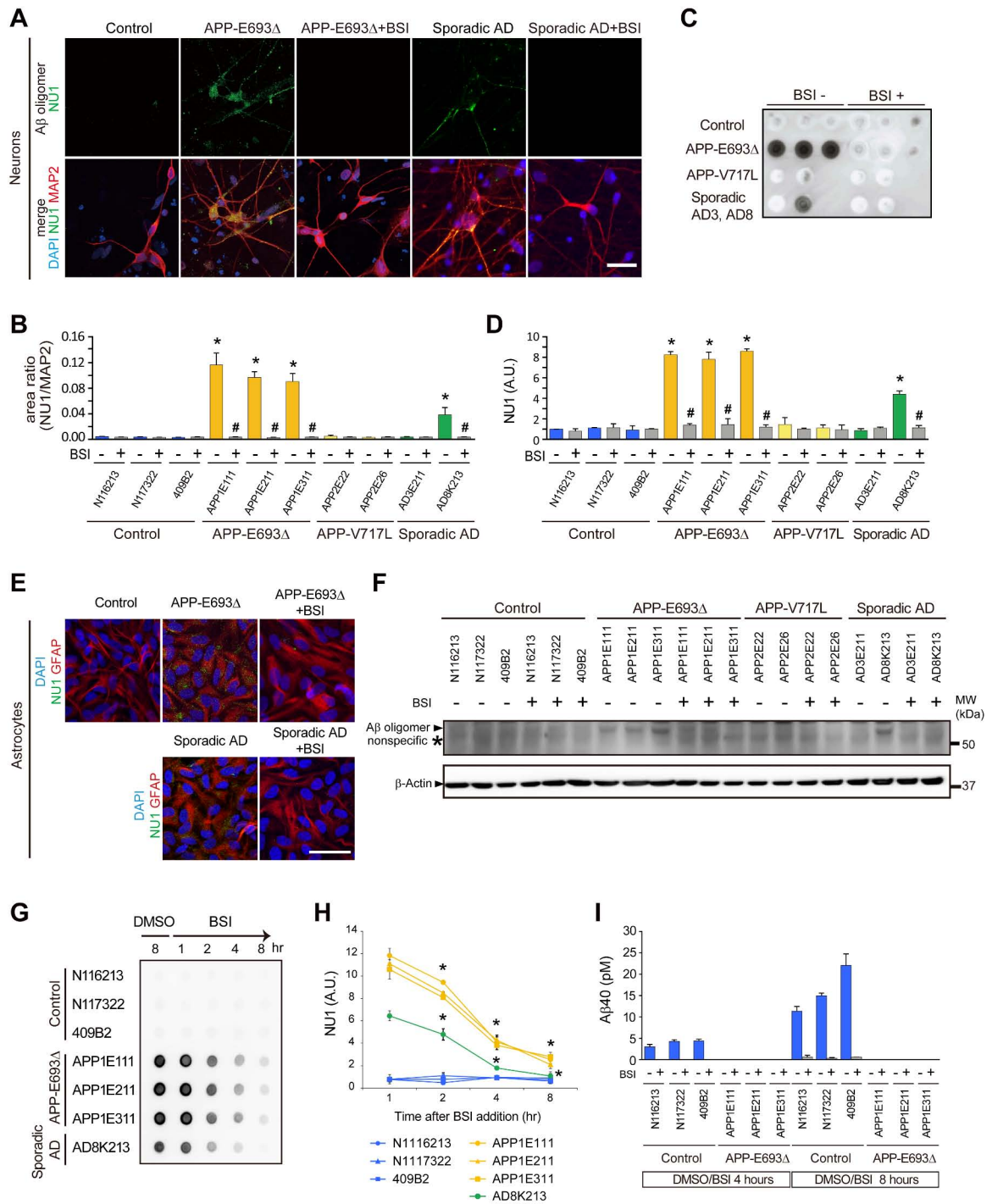


Figure 3

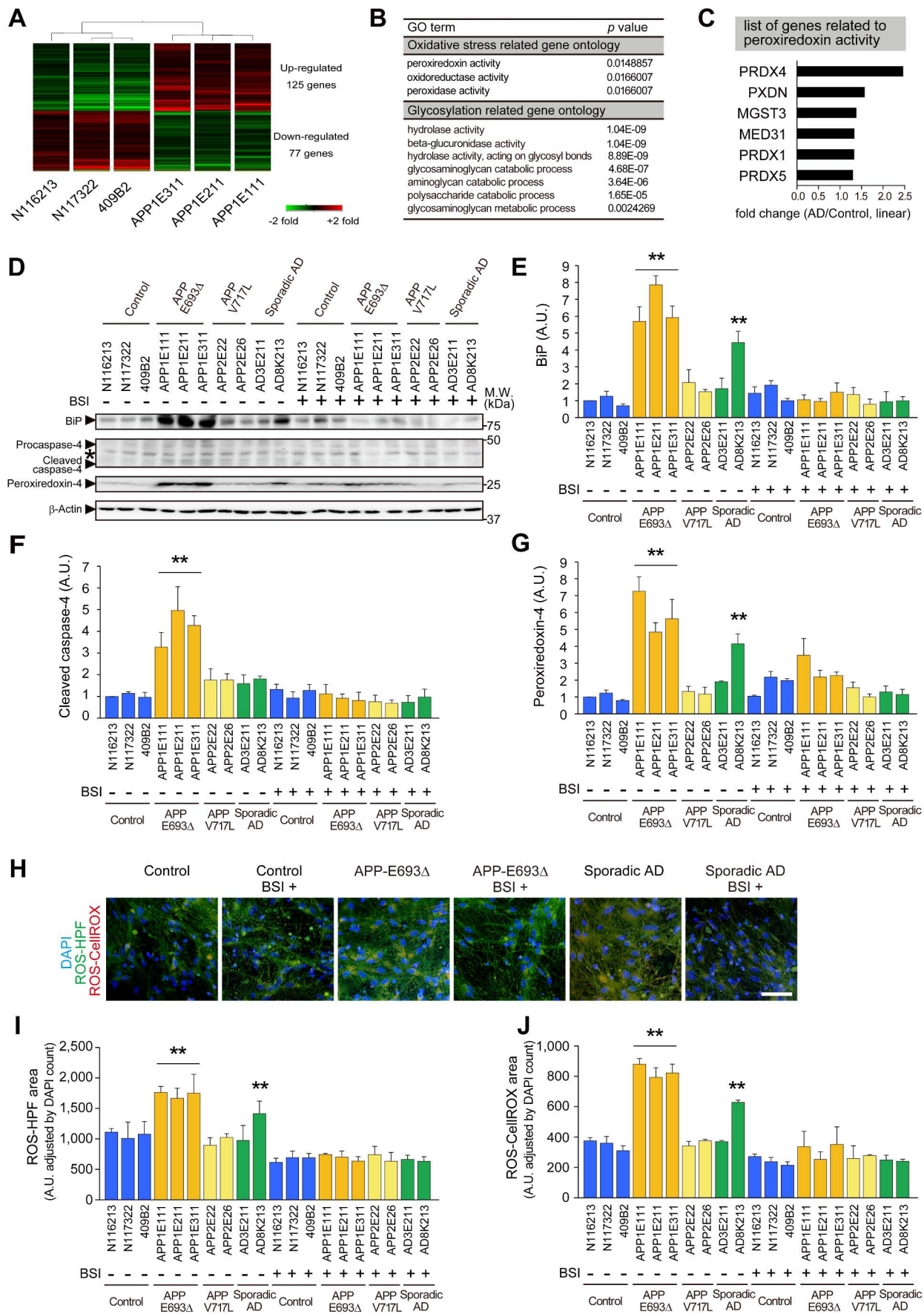
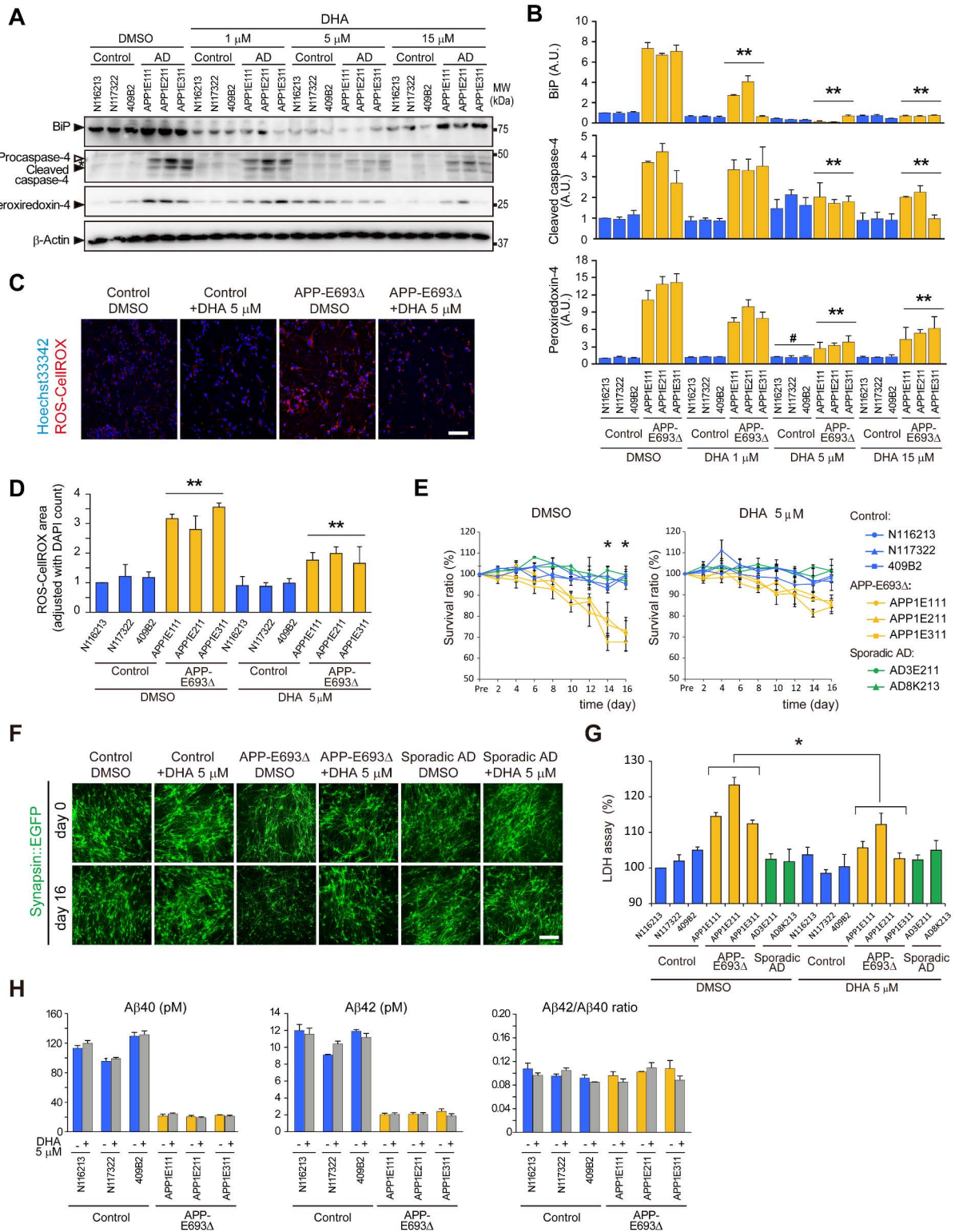


Figure 4



## **Modeling Alzheimer's Disease with iPSCs Reveals Stress Phenotypes Associated with Intracellular A $\beta$ and Differential Drug Responsiveness**

Takayuki Kondo, Masashi Asai, Kayoko Tsukita, Yumiko Kutoku, Yutaka Ohsawa, Yoshihide Sunada, Keiko Imamura, Naohiro Egawa, Naoki Yahata, Keisuke Okita, Kazutoshi Takahashi, Isao Asaka, Takashi Aoi, Akira Watanabe, Kaori Watanabe, Chie Kadoya, Rie Nakano, Dai Watanabe, Kei Maruyama, Osamu Hori, Satoshi Hibino, Tominari Choshi, Tatsutoshi Nakahata, Hiroyuki Hioki, Takeshi Kaneko, Motoko Naitoh, Katsuhiko Yoshikawa, Satoko Yamawaki, Shigehiko Suzuki, Ryuji Hata, Shu-ichi Ueno, Tsuneyoshi Seki, Kazuhiro Kobayashi, Tatsushi Toda, Kazuma Murakami, Kazuhiro Irie, William L. Klein, Hiroshi Mori, Takashi Asada, Ryosuke Takahashi, Nobuhisa Iwata, Shinya Yamanaka, and Haruhisa Inoue

Corresponding author 1

Haruhisa Inoue

email: haruhisa@cira.kyoto-u.ac.jp

Corresponding author 2

Nobuhisa Iwata

email: iwata-n@nagasaki-u.ac.jp

### **SUPPLEMENTAL FIGURES**

Figure S1 (related to Figure 1): Characterization of iPSCs and neuronal cells derived from iPSCs.

Figure S2 (related to Figure 2): Analysis of intracellular accumulation of A $\beta$  oligomers in AD fibroblasts, iPSC-derived neurons and iPSC-derived astrocytes.

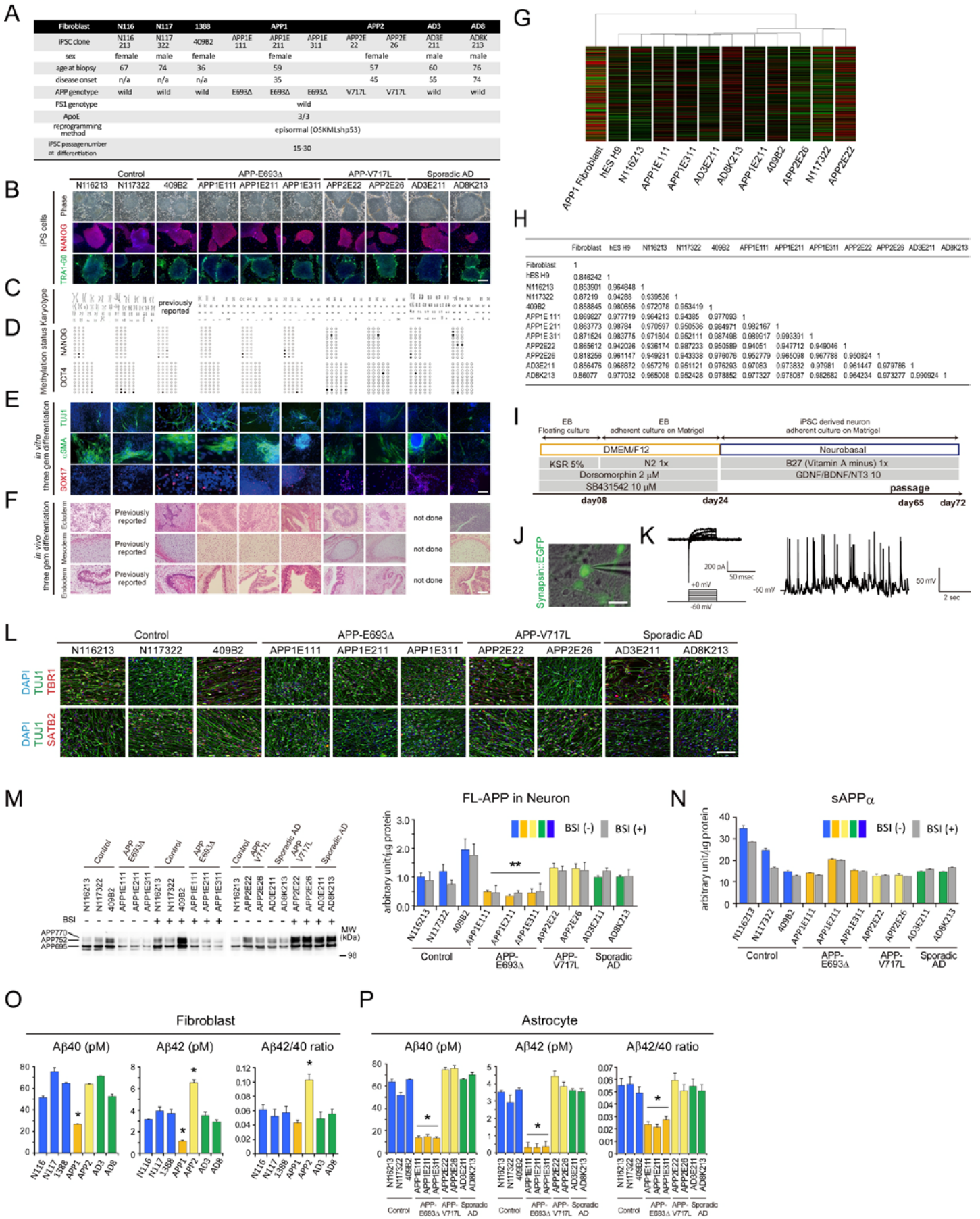
Figure S3 (related to Figure 3): Analysis of cellular stress responses in AD fibroblasts and astrocytes.

Figure S4 (related to Figure 4): Drug evaluation in relation to improvement in ER stress and A $\beta$  oligomer accumulation.

Table S1 (related to Figure 3): Changes in gene-expression between control and AD iPSC-derived neural cells and Gene ontology (GO) analysis

Table S2 (related to Figure 4): Summary of iPSC clones and their phenotypes.

# Figure S01



## Supplementary Figure S1 (related to Figure 1): Characterization of iPSCs and neuronal cells derived from iPSCs.

(A) Summary of iPSC clones. (B) Morphology and expression of human embryonic stem cell markers. iPSCs from both control and AD patients showed ES-like morphology (Phase image) and expressed pluripotent stem cell markers, NANOG and TRA1-60. Scale bar: 200  $\mu\text{m}$ . (C) iPSCs from both control and AD patients showed a normal karyotype. (D) Bisulfite genomic sequencing of the promoter regions of *NANOG* and *OCT4*. Open and closed circles indicate unmethylated and methylated CpGs, respectively. CpGs of both *NANOG* and *OCT4* promoters in all iPSC clones were demethylated. (E) *In vitro* differentiation of established iPSCs to representative three-germ layer: TUJ1 (ectoderm),  $\alpha\text{SMA}$  (mesoderm) and SOX17 (endoderm). Scale bar: 50  $\mu\text{m}$ . (F) *In vivo* (teratoma) differentiation with evidence of all three germ layers: cartilage (mesoderm), gut-like epithelium (endoderm), and neural tube-like tissues (ectoderm). Scale bar: 50  $\mu\text{m}$ . (G) Hierarchical clustering showing that the global gene expression profiles of control and AD hiPSCs are similar to human embryonic stem cells (H9) and different from human fibroblasts. (H) Pearson's correlation coefficient of each global gene profile. (I) Schematic diagram showing the differentiation protocol of cortical neurons. (J) A typical recorded neuron identified using Synapsin::EGFP. Scale bar: 50  $\mu\text{m}$ . (K, left panel) Whole-cell voltage-clamp recordings of  $\text{Na}^+$  (rapid inward) and  $\text{K}^+$  (slow outward) currents. Cells were held at  $-60\text{mV}$ , and voltage was increased stepwise from  $-60\text{ mV}$  to  $+30\text{ mV}$  in 10-mV intervals. (K, right panel) Current-clamp recordings of spontaneous action potentials.  $\text{Na}^+/\text{K}^+$  currents and action potentials were measured to examine whether iPSC-derived neurons were functionally active. In 20 EGFP-positive neurons, 95% ( $n=19$ ) presented  $\text{Na}^+/\text{K}^+$  currents, and 80% ( $n=16$ ) exhibited action potentials. Representative figures are shown. Inward currents, which were estimated to be spontaneous postsynaptic currents, were also recorded in 75% ( $n=15$ ) (data not shown). (L) Both control and AD iPSC-derived neurons expressed neuronal marker (TUJ1, Green) and cortical transcriptional markers (Red, including TBR1/SATB2). Scale bar: 100  $\mu\text{m}$ . (M) Full-length APP levels in cell lysates from control and AD neural cells were measured by quantitative western blot analysis. FL-APP expression levels in AD(APP-E693 $\Delta$ ) were significantly different from those in the other neural cells ( $*p < 0.001$ ). Data represent mean  $\pm$  S.D. ( $n = 3$  per group) (N) Soluble APP $\alpha$  levels in culture media from control and AD neural cells were measured by MSD electrochemiluminescence assay. Data represent mean  $\pm$  S.D. ( $n = 3$  per group) (O, P) Extracellular A $\beta$  in control and AD fibroblasts (O), and in control and AD iPSC-derived astrocytes (P), were measured and the A $\beta$ 42/A $\beta$ 40 ratio was calculated. Levels of A $\beta$ 40 and A $\beta$ 42 in AD(APP-E693 $\Delta$ ) fibroblasts were significantly lower than those of the others ( $*p < 0.001$ ), and levels of A $\beta$ 42 and the ratio of A $\beta$ 42/A $\beta$ 40 in AD(APP-V717L) were significantly higher than those of the others ( $*p < 0.006$ ). A $\beta$ 40 and A $\beta$ 42 levels and the ratio of A $\beta$ 42/A $\beta$ 40 in AD(APP-E693 $\Delta$ ) astrocytes are significantly lower than those of the others ( $*p < 0.001$ ). Data represent mean  $\pm$  S.D. ( $n = 3$  per group)

# Figure S02

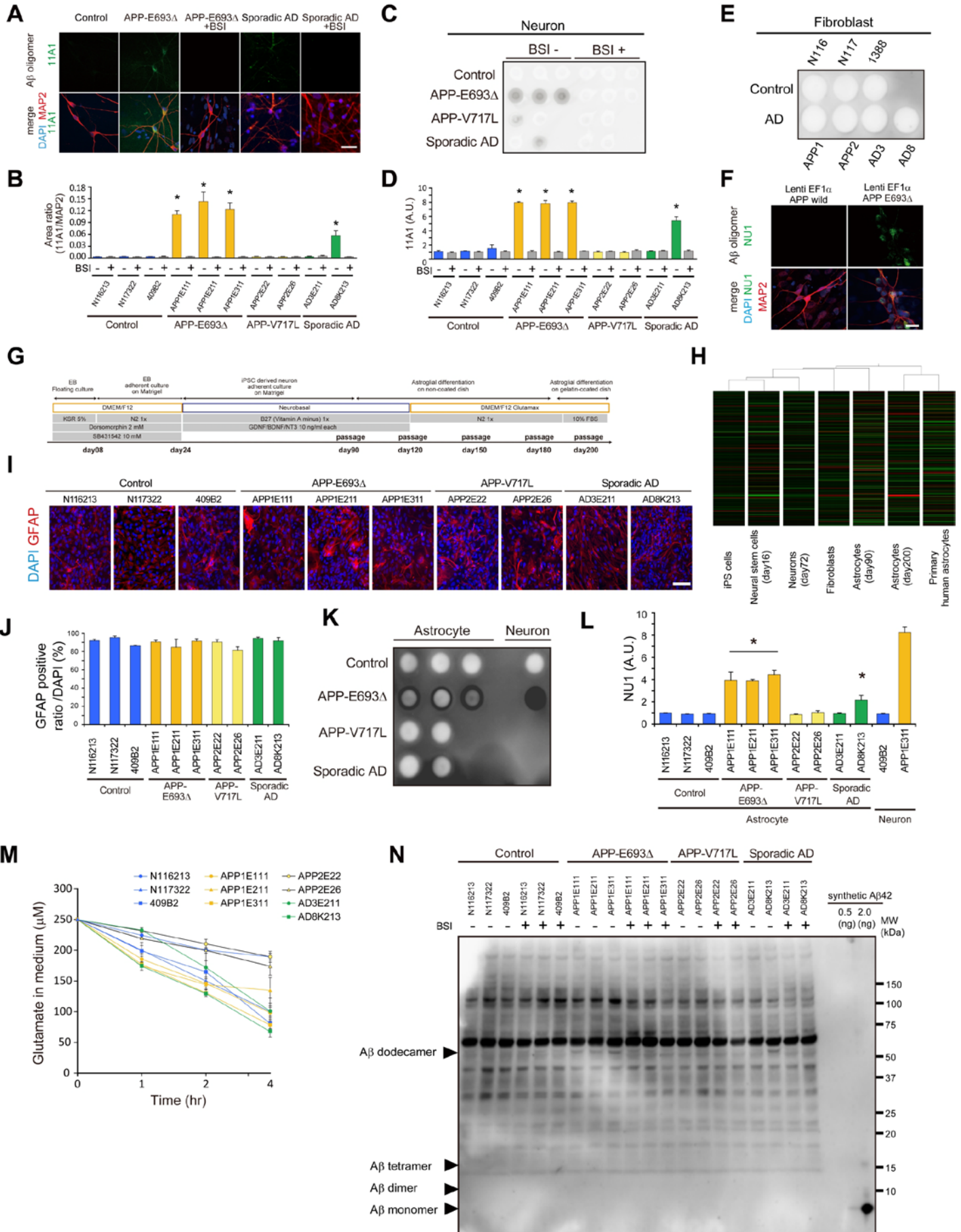
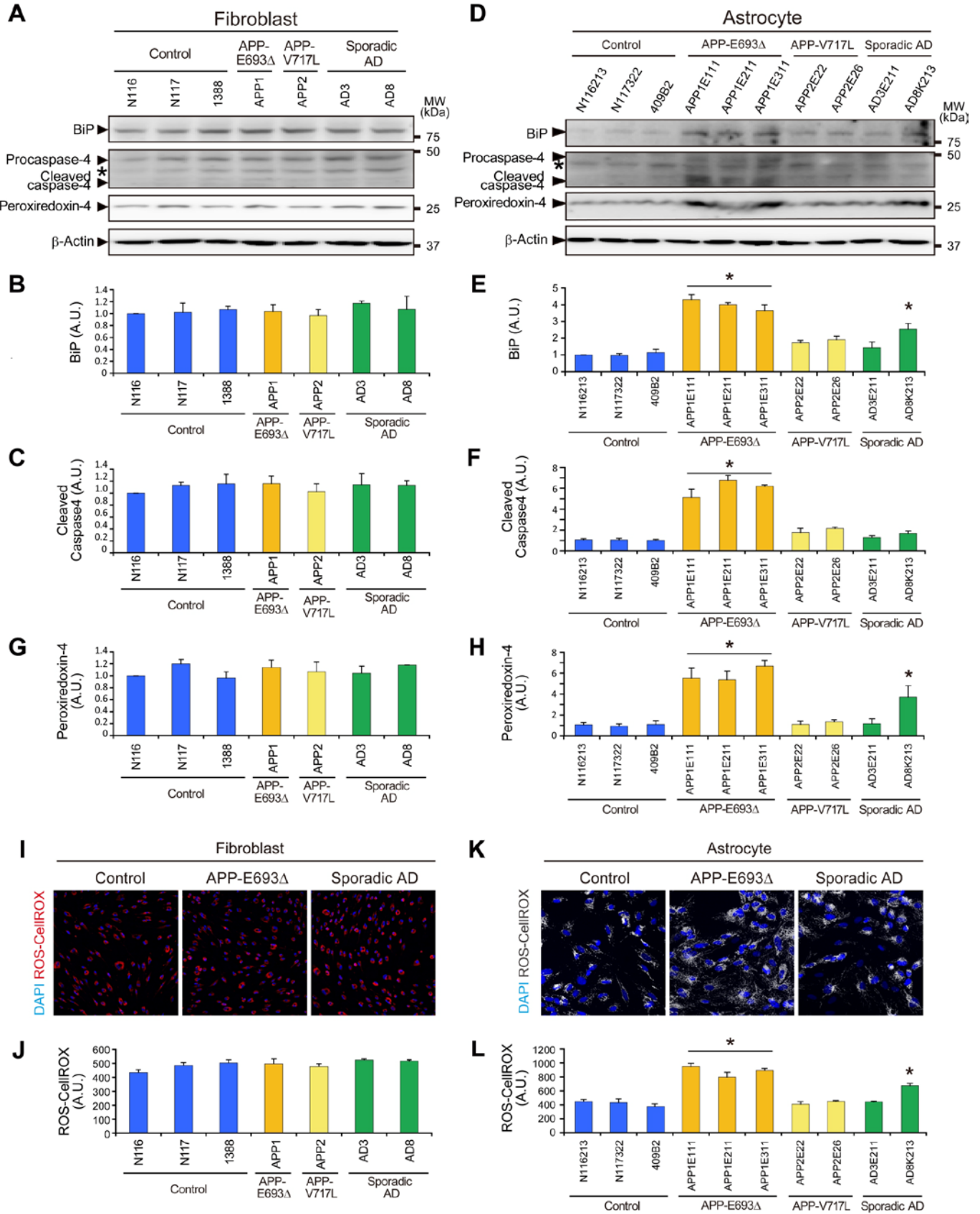


**Figure S2 (related to Figure 2): Analysis of intracellular accumulation of A $\beta$  oligomers in AD fibroblasts, iPSC-derived neurons and iPSC-derived astrocytes.**

(A) Intracellular A $\beta$  oligomer accumulation in iPSC-derived neurons (Red, MAP2-positive cells) was detected by anti-A $\beta$  oligomer monoclonal antibody 11A1 (Green) with a punctate pattern. A $\beta$  oligomer accumulation was massive in AD(APP-E693 $\Delta$ ) neurons, but only faint in control neurons. Treatment with 1  $\mu$ M BSI decreased A $\beta$  oligomer accumulation in AD neurons. DAPI staining (Blue). Scale bar: 30  $\mu$ m. (B) Quantification of A $\beta$  oligomer accumulation in panel A; ratio of the 11A1-positive area in the MAP2-positive area was analyzed. Data represent mean  $\pm$  S.D. (n = 3 per group). Levels of A $\beta$  oligomers in AD(APP-E693 $\Delta$ ) and sporadic AD(AD8K213) neurons without BSI were significantly different from those of the other neurons (\*  $p < 0.001$ ). (C) Dot-blot analysis using anti-A $\beta$  oligomer antibody 11A1. Control (N116213, N117322, 409B2), APP-E693 $\Delta$ (APP1E111, APP1E211, APP1E211), APP-V717L (APP2E22, APP2E26), sporadic AD (AD3E211, AD8K213) are dotted from the left. Blank is RIPA buffer only. (D) Signals of blots in panel C were quantified. Data represent mean  $\pm$  S.D. (n = 3 per group). BSI treatment (1  $\mu$ M) decreased A $\beta$  oligomers in AD neural cells. Levels of A $\beta$  oligomers in AD(APP-E693 $\Delta$ ) and sporadic AD(AD8K213) neural cells without BSI differed significantly from those of the other neural cells (\* $p < 0.005$ ). Data represent mean  $\pm$  S.D. (n = 3 per group) (E) A $\beta$  oligomers were not accumulated in control and AD fibroblasts. (F) Control neurons, transduced APP with lentivirus expressing APP-E693 $\Delta$  under control of EF1 $\alpha$  promoter, presented intracellular A $\beta$  oligomer formation. Intracellular A $\beta$  oligomer accumulation in iPSC-derived neurons (Red, MAP2-positive cells) was detected by anti-A $\beta$  oligomer antibody NU1 (Green, dot-like pattern). A $\beta$  oligomer accumulation was massive in the mutant APP transduction, but only faint in wild-type APP. Scale bar: 30  $\mu$ m. (G) Schematic procedures for astroglial differentiation. (H) Hierarchical clustering analysis of fibroblasts, iPSCs, primary astrocytes, and differentiated neural stem cells and astrocytes. (I) Estimation of astroglial differentiation from control and AD-iPSCs. After 180 days of differentiation, astrocytes were immunostained with an antibody against GFAP. Scale bar: 100  $\mu$ m. (J) Proportions of GFAP-positive cells in control and AD-iPSCs. Data represent mean  $\pm$  S.D. (n = 3 per clone). (K) Dot-blot analysis using anti-A $\beta$  oligomer antibody NU1. Cell lysates of control (N116213, N117322, 409B2), APP-E693 $\Delta$ (APP1E111, APP1E211, APP1E211), APP-V717L (APP2E22, APP2E26), and sporadic AD (AD3E211, AD8K213) astrocytes were dotted from the left. Blank is RIPA buffer only. (L) Signals of blots in panel F were quantified. Data represent mean  $\pm$  S.D. (n = 3 per group). Levels of A $\beta$  oligomers in AD(APP-E693 $\Delta$ ) and sporadic AD(AD8K213) astrocytes were significantly different from those of the other astrocytes (\* $p < 0.001$ ). (M) Assay of glutamate transport in control and AD astrocytes. Data represent mean  $\pm$  S.D. (n = 3 per group). (N) Full western blot of A $\beta$  oligomers (dodecamers) in control and AD neural cells in the presence or absence of BSI.

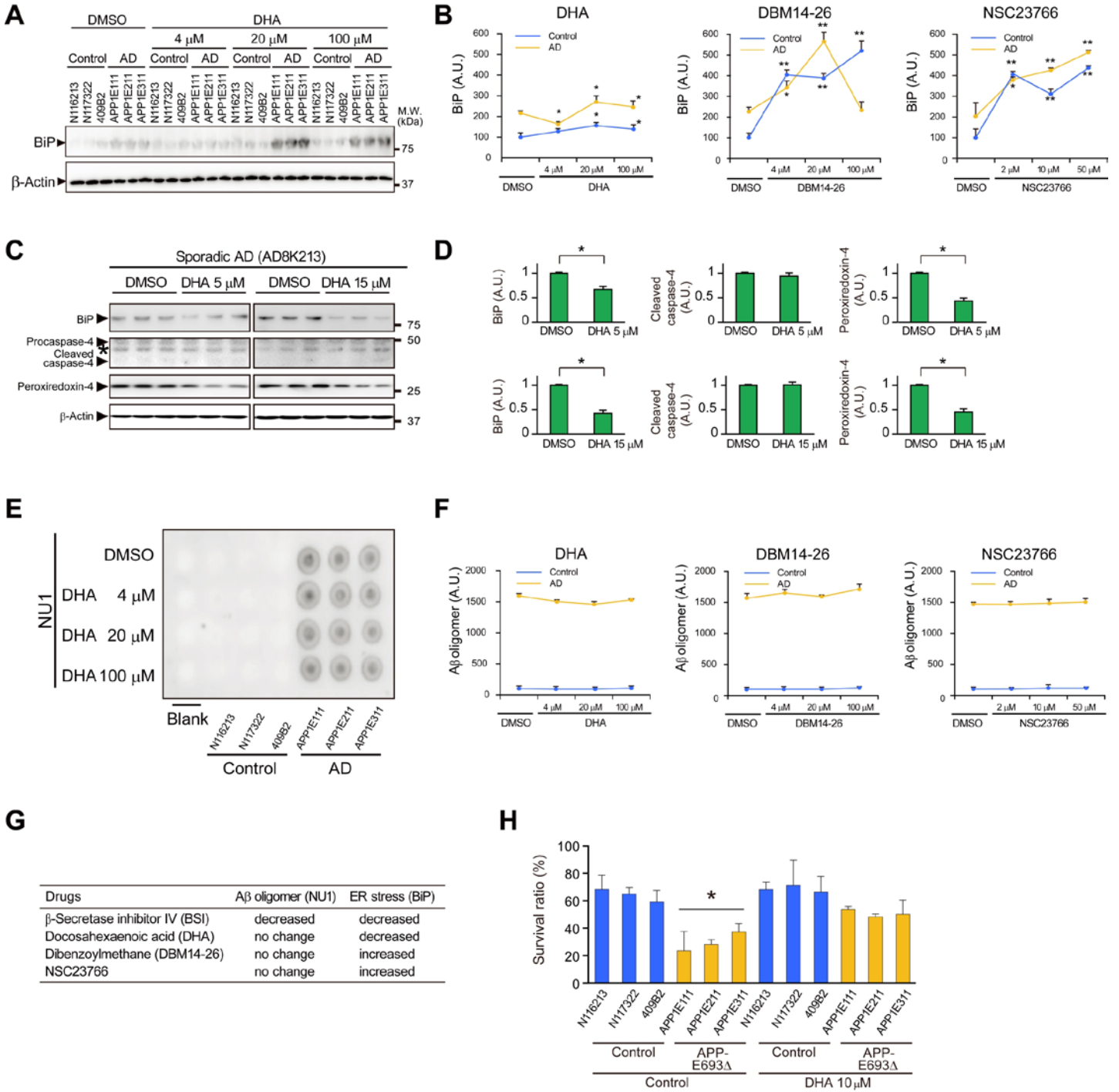
Figure S03



**Supplementary Figure S3 (related to Figure 3): Analysis of cellular stress responses in AD fibroblasts and astrocytes.**

(A) Western blot analysis of ER stress markers (BiP, caspase-4), peroxiredoxin-4, and reference protein ( $\beta$ -actin) in lysates from control and AD fibroblasts. (B, C) Densitometric analysis of BiP protein (B) and cleaved caspase-4 (C) in panel A. Their measured values were normalized by that of  $\beta$ -actin. Data represent mean  $\pm$  S.D. (n = 3 per group). (D) Western blot analysis of ER stress markers (BiP, caspase-4) and reference protein ( $\beta$ -actin) in lysates from control and AD astrocytes. (E, F) Densitometric analysis of BiP protein (E) and cleaved caspase-4 (F) in panel D. Their measured values were normalized by that of  $\beta$ -actin. Data represent mean  $\pm$  S.D. (n = 3 per group). Levels of ER stress markers in the AD(APP-E693 $\Delta$ ) astrocytes were significantly different from those of the others ( $*p < 0.001$ ). Levels of BiP in the sporadic AD(AD8K213) astrocytes were significantly different from those of the others ( $*p < 0.001$ ). (G) Densitometric analysis of peroxiredoxin-4 in panel A. Their measured values were normalized by that of  $\beta$ -actin. Each column represents mean  $\pm$  S.D. (n = 3 per group). (H) Densitometric analysis of peroxiredoxin-4 in panel D. Their measured values were normalized by that of  $\beta$ -actin. Each column represents mean  $\pm$  S.D. (n = 3 per group). Levels of peroxiredoxin-4 in the AD(APP-E693 $\Delta$ ) and the sporadic AD(AD8K213) astrocytes were significantly different from those of the others ( $*p < 0.001$ ). (I) Typical images of ROS detected by ROS-HFF and Hoechst33342 staining of control and AD fibroblasts with or without BSI treatment. Scale bar: 30  $\mu$ m. (J) Quantitative data of panel I. Each value is shown as a ratio of the ROS-stained area, adjusted with DAPI counts. Data represent mean  $\pm$  S.D. (n = 3 per group). (K) Typical images of ROS detected by ROS-CellROX and Hoechst33342 staining of control and AD fibroblasts with or without BSI treatment. Scale bar: 30  $\mu$ m. (L) Quantitative data of panel K. Each value indicates a ratio of the ROS-stained area, adjusted with DAPI counts. Data represent mean  $\pm$  S.D. (n = 3 per group). Levels of ROS in AD(APP-E693 $\Delta$ ) and sporadic AD(AD8K213) astrocytes were significantly different from those of the others ( $*p < 0.001$ ).

# Figure S04



**Supplementary Figure S4 (related to Figure 4): Drug evaluation in relation to improvement in ER stress and A $\beta$  oligomer accumulation.**

(A) After treatment with vehicle or DHA at indicated concentrations, cells were lysed and subjected to immunoblot analysis with antibodies of an ER stress marker (BiP) and a reference protein ( $\beta$ -actin) (DHA concentration: 4, 20 and 100  $\mu$ M) (B) Densitometric analysis of ER stress markers with or without drug treatment: 1) DHA, 2) DBM14-26, 3) NSC23766. Data represent mean  $\pm$  S.D. (n = 3 per group). Measured values were normalized by that of  $\beta$ -actin. Data represent mean  $\pm$  S.D. (n = 3 per group, per each concentration). (C) Sporadic AD(AD8K213) neural cells at day 72 were treated with vehicle or DHA at indicated concentrations for 48 h. Then, cells were lysed and subjected to immunoblot analysis with antibodies of ER stress markers (BiP, casapase-4), peroxiredoxin-4 and a reference protein ( $\beta$ -actin) (DHA concentration: 5 and 15  $\mu$ M). (D) Densitometric analysis of ER stress markers and peroxiredoxin-4 in panel C. Measured values were normalized by that of  $\beta$ -actin. Each column represents mean  $\pm$  S.D. (n = 3 per group) (\* $p$  < 0.005). (E) Dot-blot analysis using NU1 antibody, after treatment with vehicle or DHA at indicated concentrations. (F) Densitometric analysis of dot-blot analysis using NU1 antibody, with or without drug treatment. Data represent mean  $\pm$  S.D. (n = 3 per group). (G) Summary of effects of drugs. (H) Treatment with 10  $\mu$ M DHA (n = 3) for 48 h blocked hydrogen peroxide (200  $\mu$ M)-induced death of AD neurons. Data represent mean  $\pm$  S.D. (n = 3 per group). The control group of AD(APP-E693 $\Delta$ ) neural cells was significantly different from the other groups (\* $p$  < 0.005).

**Supplementary Table S1 (related to Figure 3): Changes in gene-expression between control and AD iPSC-derived neural cells and Gene ontology (GO) analysis**

(a) List of genes showing significantly different expression (fold change > 1.5,  $p < 0.05$ ) between control and AD iPSC-derived neural cells. Up- or down-regulated genes were shown each in red or blue color. (b) List of GO terms from the gene datasets of Table S1 (a), using Gene spring software.

(All data is contained in Supplementary spread sheet file.)

Phenotype		APP E693Δ (APP1E 111 211, 311)	APP V717L (APP2E 22, 26)	Sporadic AD 1 (AD3E 211)	Sporadic AD 2 (AD8K 213)
Intracellular Aβ oligomer		++	-	-	+
Cellular stress	BiP	↑↑	→	→	↑
	PRDX4	↑↑	→	→	↑
	Caspase-4 (activated type)	↑	→	→	→
	ROS	↑↑	→	→	↑
Survival rate		↓	→	→	→

**Supplementary Table S2 (related to Figure 4): Summary of iPSC clones and their phenotypes.**

Intracellular A $\beta$  oligomers, cellular stresses and survival rates of iPSC clones.

+, accumulated; -, not detected;  $\uparrow$ , increased;  $\downarrow$ , decreased;  $\rightarrow$ , no significant change.

## SUPPLEMENTAL EXPERIMENTAL PROCEDURES

### Karyotyping and genotyping

Karyotyping was performed in our institute. Genotyping of *APP* single nucleotide mutation was performed by PCR amplification of genomic DNA and directly sequenced (3100 Genetic Analyzer; Applied Biosystems, Life Technologies). *APOE* gene was amplified by PCR (forward primer TCC AAG GAG CTG CAG GCG GCG CA; reverse primer ACA GAA TTC GCC CCG GCC TGG TAC ACT GCC A). The PCR products were digested by *HhaI* at 37°C for 2 h and then subjected to electrophoresis to analyze band size.

### *In vitro* Differentiation

hiPSCs were harvested by treatment with CTK solution and used for embryoid body (EB) formation. Clumps of cells were transferred to petri dishes in DMEM/F12 containing 20% knockout serum replacement (KSR; Life Technologies), 2 mM L-glutamine, 0.1 M nonessential amino acids, 0.1 M 2-mercaptoethanol (Life Technologies), and 0.5% penicillin and streptomycin. The medium was changed every other day. For spontaneous differentiation, 8-day-old EBs were plated onto gelatin-coated coverslips and allowed to differentiate in DMEM + 10% fetal bovine serum for an additional 8 days.

### Generation of hiPSC-derived teratomas

Undifferentiated hiPSCs were harvested by CTK solution and the pellets were suspended in DMEM/F12. The cells were subcutaneously transplanted into NOG mice (Central Institute for Experimental Animals, Japan). Eight weeks after injection, tumors were dissected and fixed with PBS containing 4% formaldehyde. Paraffin-embedded tissue was sliced and stained with hematoxylin/eosin.

### Bisulfite Genomic Sequencing

Genomic DNA (1 µg) from iPS cells was processed for bisulfite modification using an EZ DNA methylation Gold Kit (Zymo Research Corporation). One conserved CpG-enriched region in the *Oct-4* promoter and one conserved CpG-enriched region in the *NANOG* promoter were selected for amplification by PCR with *ExTaq* Hot start version (TaKaRa Bio, Japan). The PCR products were subcloned into pCR4 vector (Life Technologies). Ten clones of each sample were verified by sequencing with Sp6 universal primer. All primer sequences were as follows: Oct4-3F ATT TGT TTT TTG GGT AGT TAA AGG T; Oct4-3R CCA ACT ATC TTC ATC TTA ATA ACA TCC; NANOG\_BS-F TGG TTA GGT TGG TTT TAA ATT TTT G; NANOG\_BS-R AAC CCA CCC TTA TAA ATT CTC AAT TA.

### Microarray analysis for iPSCs

Total RNA from HDF and hiPSCs was labeled with Cy3. Samples were hybridized with Whole Human Genome Microarray 4 Å~44K (G4112F, Agilent Technologies). Each sample was hybridized once with the one-color protocol. Arrays were scanned with a G2565BA Microarray Scanner System (Agilent Technologies). Data were analyzed by GeneSpring GX7.3.1 software (Agilent Technologies).

### Induction of cortical neuron differentiation

hiPSCs were dissociated to single cells and quickly reaggregated in U-bottom 96-well plates for suspension culture (Greiner Bio-One), pre-coated with 2% Pluronic F-127 (Sigma-Aldrich) in 100% ethanol (Supplementary Figure S3A). Aggregations, embryoid bodies (EB), were cultured in 'DFK5% medium' (DFK5%; DMEM/Ham's F12 (Gibco, USA) supplemented with 5%

KSR (Gibco), NEAA (Invitrogen), L-glutamine (Sigma-Aldrich), 0.1 M 2-mercaptoethanol (Invitrogen)) with or without 2  $\mu$ M dorsomorphin (Sigma-Aldrich) and 10  $\mu$ M SB431542 (Cayman Chemical) in a neural inductive stage (day 00 to 08). After neural induction, EB were transferred onto Matrigel (Becton Dickinson)-coated 6-well culture plates and cultured in DFK5% supplemented with 1x N2 supplement (Invitrogen), 2  $\mu$ M dorsomorphin, and 10  $\mu$ M SB431542 in the patterning stage (day 08 to 24). A large number of neural precursor cells (NESTIN-positive) were observed to migrate from the EB core. After the patterning stage, migrated neural precursor cells were separated from the plate bottom using Accutase (Innovative Cell Technologies, Inc.) and cultured in Neurobasal medium FULL, Neurobasal<sup>®</sup> Medium (Invitrogen/Gibco) supplemented with 1x B27 without Vitamin A (Invitrogen/Gibco), 1x Glutamax (Invitrogen/Gibco), 10 ng/ml BDNF, 10 ng/ml GDNF and 10 ng/ml NT-3 on Matrigel-coated 24-well culture plates or cover-slip in the neural maturation stage (day 24 to 72).

### Electrophysiological recordings

Whole-cell patch-clamp recordings were performed from iPSC-derived neurons expressing Synapsin::EGFP by lentivirus vector under fluorescence microscopy in combination with differential interference contrast imaging. The recording micropipettes were filled with intracellular solution consisting of 140 mM KCl, 2 mM MgCl<sub>2</sub>, 10 mM HEPES, and 1 mM EGTA, adjusted to pH 7.4 with NaOH. Cells were maintained at 30°C during the experiment, and were continuously superfused with oxygenated Krebs-Ringer solution consisting of 125 mM NaCl, 2.5 mM KCl, 1.25 mM NaH<sub>2</sub>PO<sub>4</sub>, 26 mM NaHCO<sub>3</sub>, 1 mM MgCl<sub>2</sub>, 2 mM CaCl<sub>2</sub>, and 20 mM glucose. Voltage-clamp and current-clamp recordings were made using an EPC 9 amplifier (HEKA Elektronik, Lambrecht) and data were analyzed with Patchmaster software (HEKA).

### Production of VSV-G-pseudotyped lentivirus

EF1 $\alpha$  (kind gift from Dr. Akitsu Hotta) or Synapsin I promoter was inserted into pENTR1A vector (Invitrogen). The production of VSV-G-pseudotyped lentivirus was performed as reported previously (Hioki et al. 2007). Briefly, the viral plasmid carrying a gene was cotransfected with a mixture of packaging plasmids (pLP1, pLP2 and pLP/VSVG; Invitrogen) into the 293FT producer cell line (Invitrogen), using Lipofectamine 2000 (Invitrogen). Sixty hours after transfection, the viral particles in the culture supernatant were collected and filtered through 0.45- $\mu$ m filters (Millipore, Corning).

### Immunocytochemistry

Cells were fixed in 4% paraformaldehyde (pH 7.4) for 30 min at room temperature and rinsed with PBS. The cells were permeabilized in PBS containing 0.2% Triton X-100 for 10 min at room temperature, followed by rinsing with PBS. Nonspecific binding was blocked with PBS containing 10% donkey serum for 60 min at room temperature. Cells were incubated with primary antibodies overnight at 4°C, and then labeled with appropriate fluorescent-tagged secondary antibodies. DAPI (Life Technologies) was used to label nuclei. Fluorescence images were acquired on an FV1000 laser-scanning confocal microscope (OLYMPUS) or LSM710 microscope (Carl Zeiss). The following primary antibodies were used in immunocytochemistry: NANOG (1:10 dilution; R&D Systems), TRA1-60 (1:400; Cell Signaling Technology),  $\alpha$ SMA (1:1,000; DAKO), SOX17 (1:200; Millipore), TUJ1 (1:4,000; Chemicon), CTIP2 (1:400; Abcam), SATB2 (1:800; Abcam), TBR1 (1:800; Abcam), NU1 (1:100), MAP2 (1:1,000; Millipore), BiP (1:400; Millipore), GFAP (1:2,000; DAKO) and 11A1 (1:400; IBL, Japan). 3'-(p-hydroxyphenyl) fluorescein (HPF) (Sekisui Medical, Japan) or CellROX deep red reagent (Invitrogen) was used to image intracellular ROS according to the manufacturer's protocol. For evaluating the positive count ratio of immunocytochemistry, we imaged the cells using automated microscopy by IN CELL Analyzer 2000 (GE Healthcare) and then counted the immunostained structures by using IN CELL Developer toolbox software 1.9 (GE Healthcare).

## Immunoblots

Cells were lysed in RIPA buffer (50 mM Tris-HCl buffer, pH 8.0, 150 mM NaCl, 1% NP-40, 0.5% deoxycholate, 0.1% SDS, and protease inhibitor cocktail (Roche Diagnostics)). Each 5-, 10- or 20- $\mu$ g sample of protein was subjected to SDS-PAGE (5-20% gradient SDS-polyacrylamide gels, ATTO Co.), and separated proteins were transferred to polyvinylidene fluoride membrane (Hybond<sup>TM</sup>-P, GE Healthcare) or nitrocellulose membrane (PROTRAN; 0.2  $\mu$ m pore-size, Whatman). The membranes were incubated with primary antibodies, followed by appropriate secondary antibodies, and then visualized using ECL plus or ECL prime (GE Healthcare). For dot-blot analysis, cell lysate samples (each 2 or 4  $\mu$ g/spot) were loaded on a nitrocellulose membrane. The membranes were incubated with primary antibodies, followed by appropriate secondary antibodies, and then visualized using ECL prime (GE Healthcare). The images were acquired on LAS 4000 (GE Healthcare). The intensity of the protein band or spot was analyzed using Science Laboratory 2001 Image Gauge software (GE Healthcare). Each set of experiments was repeated at least two times to confirm the results. The following primary antibodies were used: NU1 (1:1,000), 6E10 (1:3,000), BiP (1:7,500; Abcam), caspase-4 (1:3,000, MBL), peroxiredoxin-4 (1:6,000, Abcam) and  $\beta$ -actin (1:20,000, MBL).

## Extracellular A $\beta$ measurement using electrochemiluminescence assays

A $\beta$  species and sAPP $\beta$  in culture media were measured by Human (6E10) A $\beta$  3-Plex Kit and sAPP $\beta$  Kit (Meso Scale Discovery). For A $\beta$  species, this assay uses 6E10 antibody to capture A $\beta$  peptide and SULFO-TAG-labeled different N-terminus specific anti-A $\beta$  antibodies for detection by electrochemiluminescence with Sector<sup>®</sup> Imager 6000 (Meso Scale Discovery). Each sample was measured in duplicate, and the mean was adopted.

## Intracellular A $\beta$ measurement using sandwich ELISA

At day 72 from neuronal differentiation, two-day incubated conditioned media were collected from cultured neuronal cells ( $2 \times 10^5$  cells) and centrifuged at 4,000 g for 10 min. The resultant clear supernatants were added to 6 M guanidine solution containing 50 mM Tris-HCl, protease inhibitor cocktail Complete<sup>®</sup> (Roche Diagnostics) and 0.7  $\mu$ g/ml pepstatin A (Peptide Institute, Japan) (pH 7.6) to give 0.5 M (final concentration), and then sonicated before application to ELISA as an extracellular fraction. The cells were washed twice with ice-cold PBS, collected with a cell scraper, and sonicated in 6 M guanidine solution. The cell lysate was diluted 12 times to reduce the concentration of guanidine and was then used as intracellular or cell-associated fraction. The samples were subjected to sandwich ELISA (Immuno-Biological Laboratories Co.) with a combination of monoclonal antibodies specific to the N-terminal of A $\beta$  and specific to the C-terminal of A $\beta$ 40 or A $\beta$ 42, to determine the amounts of secreted A $\beta$ . We also examined the effect of BACE1 inhibitor IV (Merck) on A $\beta$  oligomer levels. All media were replaced with new media containing 1  $\mu$ M BACE1 inhibitor IV, and two-day conditioned media were analyzed as described above.

## Astroglial differentiation

At day 90 from neuronal differentiation, iPS-derived neuronal cells were plated at  $40 \times 10^5$  cells per 6-cm dish without coating in Neurobasal medium FULL (described above). After passage, neurons could not attach to a non-coated polystyrene dish surface or they died by anoikis. Astroglia, on the other hand, could attach and proliferate. By repeated passage in the same manner at days 120, 150 and 180, astroglia increased their own abundance ratio and showed positive GFAP-immunostaining (more than 80%). After day 200 from neuronal differentiation, culture medium was changed to DMEM/F12 Glutamax

(Invitrogen/Gibco) with 10% FBS (Invitrogen/Gibco) and astroglial cells were used for assay or stocked in a -80°C deep-freezer. Human primary astrocytes were purchased from Lonza as control cells for astrocyte differentiation.

#### Glutamate clearance assay

Differentiated astroglial cells were replated at  $4 \times 10^4$  cells per well in 48-well plates coated with 0.1% gelatin. Three days after replating, L-glutamate (final concentration 250  $\mu$ M) (Nacalai, Japan) was added to assess glutamate uptake. To measure extracellular glutamate concentrations, Glutamate Assay Kit colorimetric assay II (Yamasa Corporation, Tokyo, Japan) was used. We added an equivalent amount of glutamate (250  $\mu$ M concentration) to iPSC-derived astrocyte culture medium and calculated glutamate uptake at 1-4-hour time points.

#### Microarray analysis for differentiated neural cells

Total RNA from differentiated neural cells was extracted by RNeasy mini kit (QIAGEN) and altered into fragmented/biotinylated cDNA by Ovation Pico WTA System/ Encore Biotin Module kit (NuGENE). Fragmented cDNA samples were hybridized with GeneChip Human Gene 1.0 ST Array (Affymetrix). Each sample was hybridized once with the one-color protocol. Arrays were scanned with a GeneChip® Scanner 3000 7Gt (Affymetrix). Data were analyzed by GeneSpring GX7.3.1 software (Agilent Technologies).

#### Drug treatment

iPSC-derived neurons at day 72 were incubated in media containing BSI, DHA (Nacalai), DBM14-26 or Rac1 inhibitor (NSC23766, Calbiochem). All media were replaced with new media containing each drug, and iPSC-derived neurons were subjected to immunoblot analysis 48h later.

#### Neuronal Survival Analysis

At day 65 after neuronal differentiation, lentiviral vectors expressing synapsin I promoter-driven EGFP (Synapsin::EGFP) were transduced, and then plated at  $2 \times 10^5$  cells per well in 12-well plates coated with matrigel. EGFP-positive neurons were observed within five days after transduction. After confirming that the increasing number of EGFP-positive neurons had reached a stable plateau, iPSC-derived neural cells were replated at  $4 \times 10^4$  cells per well in 96-well plates coated with matrigel. Five days after replating, neurobasal medium FULL (described above) was changed to Neurobasal® Medium Minus Phenol Red (Invitrogen), without B27 supplement/Glutamax/neurotrophic factors, with or without 5  $\mu$ M DHA. EGFP-positive neurons were imaged automatically at intervals of 48 h using IN CELL Analyzer 2000. The number of EGFP-positive neurons at each time point/well was automatically counted by IN CELL Developer toolbox software 1.9. Neuronal death was determined by cell membrane rupture, blebbing, or loss of EGFP fluorescence. Neuronal survival rate was calculated with the formula 'counts at analysis/counts at start (%)'. Lactate dehydrogenase (LDH) assay was performed to assess the cytotoxic state during neuronal survival analysis. LDH, a cytoplasmic enzyme, is released into culture medium when the cell membrane is damaged. Released LDH in culture medium was measured by Cytotoxicity Detection Kit (LDH) (Roche Diagnostics). LDH levels were converted to a relative value (%), in comparison with the N116213 clone without DHA at day 16 of the survival assay.

## **SUPPLEMENTAL REFERENCES**

Hioki, H., Kuramoto, E., Konno, M., Kameda, H., Takahashi, Y., Nakano, T., Nakamura, K.C., and Kaneko, T. (2009). High-level transgene expression in neurons by lentivirus with Tet-Off system. *Neurosci Res* 63, 149-154.